# A carbonate-rich lake solution to the phosphate problem of the origin of life

Jonathan D. Toner[a,1] and David C. Catling[a]

[a]Department of Earth & Space Sciences, University of Washington, Seattle, WA 98195

Edited by Jonathan I. Lunine, Cornell University, Ithaca, NY, and approved November 27, 2019 (received for review September 16, 2019)

**Phosphate is central to the origin of life because it is a key component of nucleotides in genetic molecules, phospholipid cell membranes, and energy transfer molecules such as adenosine triphosphate. To incorporate phosphate into biomolecules, prebiotic experiments commonly use molar phosphate concentrations to overcome phosphate's poor reactivity with organics in water. However, phosphate is generally limited to micromolar levels in the environment because it precipitates with calcium as low-solubility apatite minerals. This disparity between laboratory conditions and environmental constraints is an enigma known as "the phosphate problem." Here we show that carbonate-rich lakes are a marked exception to phosphate-poor natural waters. In principle, modern carbonate-rich lakes could accumulate up to ∼0.1 molal phosphate under steady-state conditions of evaporation and stream inflow because calcium is sequestered into carbonate minerals. This prevents the loss of dissolved phosphate to apatite precipitation. Even higher phosphate concentrations (>1 molal) can form during evaporation in the absence of inflows. On the prebiotic Earth, carbonate-rich lakes were likely abundant and phosphate-rich relative to the present day because of the lack of microbial phosphate sinks and enhanced chemical weathering of phosphate minerals under relatively $CO_2$-rich atmospheres. Furthermore, the prevailing $CO_2$ conditions would have buffered phosphate-rich brines to moderate pH (pH 6.5 to 9). The accumulation of phosphate and other prebiotic reagents at concentration and pH levels relevant to experimental prebiotic syntheses of key biomolecules is a compelling reason to consider carbonate-rich lakes as plausible settings for the origin of life.**

phosphate | origin of life | early Earth | carbonate-rich lakes

Phosphate is central to the origin of life (1–4) because it is a key component of nucleotides, phospholipids, and metabolites such as adenosine triphosphate used in cellular replication, compartmentalization, and energy transfer, respectively (5). A major issue for prebiotic chemistry is that phosphate combines with $Ca^{2+}$ down to micromolar levels to form apatite-group minerals [e.g., $Ca_5(PO_4)_3(OH,F,Cl)$] or with $Fe^{3+}$ and $Al^{3+}$ in acidic solutions to form Fe/Al phosphates (6). However, laboratory experiments seeking to understand prebiotic phosphorylation (i.e., adding a phosphoryl group to an organic molecule) commonly use ∼1 molal phosphate to overcome phosphate's poor reactivity with organics in water (2–4, 7, 8). Concentrated phosphate also catalyzes acid/base and nucleophilic reactions and acts as a pH and chemical buffer (8). The geochemical difficulty of forming concentrated phosphate, combined with its central role in prebiotic syntheses, is a long-standing enigma known as "the phosphate problem" (1, 4).

Difficulties with using aqueous phosphate have motivated research on more reactive phosphorylating agents such as struvite ($MgNH_4PO_4{\cdot}6H_2O$), polyphosphates, and amidophosphates (9–11), and alternative solvents such as formamide and urea (12, 13). These approaches are generally problematic because the proposed reagents would have been scarce in plausible early Earth environments (10, 14, 15). Reduced phosphorus compounds, such as phosphite ($PO_3^{3-}$), may also form when water reacts with meteoritic material, and are more reactive and soluble than orthophosphate (1, 16); however, phosphorylation with phosphite primarily yields phosphonates, that is, compounds with P–C bonds vs. P–O–C bonds in organophosphates. These issues have motivated recent proposals for an origin of life in extremely acidic hot spring environments (17), which can accumulate aqueous phosphate as $H_3PO_4^0$ species, but measured phosphate concentrations in acid hot springs are limited to <1 mM (18).

Here we to show that carbonate-rich lakes are an exception to the rule of low phosphate concentrations found in most natural waters. Using environmental data, laboratory experiments, and geochemical models, we find that >1 molal phosphate concentrations could have occurred on the early Earth in carbonate-rich lake environments. This provides a plausible geochemical source of concentrated, soluble phosphate needed in prebiotic syntheses, and points to a specific environment for the origin of life in carbonate-rich lakes.

## High Phosphate Concentrations in Present-Day, Carbonate-Rich Lakes

Phosphate concentrations are remarkably high in closed-basin, carbonate-rich lakes and generally increase with increasing carbonate alkalinity (Fig. 1) (see *SI Appendix*, *Appendix A* for other dissolved species). Searles Lake, located within the Mojave Desert in California, is an economically important carbonate-, boron-, and sulfate-rich groundwater brine within a dry lake basin that contains 5 to 17 mM phosphate (19). Even higher total phosphorus concentrations are found in Goodenough and Last Chance Lakes in British Columbia, which can exceed 50 mM during

### Significance

**Phosphate is crucial for the origin of life because it is ubiquitous in key biomolecules. A major issue is that prebiotic syntheses use concentrated phosphate to incorporate phosphate into biomolecules, whereas natural waters are generally phosphate-poor because phosphate reacts with calcium to form low-solubility apatite minerals. Here we show that carbonate-rich lakes can concentrate phosphate to >1 molal levels by locking up calcium in carbonate minerals, which prevents phosphate removal by apatite precipitation. Phosphate-rich lakes may have preferentially formed on the prebiotic Earth because of carbonic acid weathering under $CO_2$-rich atmospheres and the absence of microbial phosphate consumption. This specifically points to an origin of life in carbonate-rich lakes, and so defines aqueous conditions that prebiotic chemists should consider.**

Author contributions: J.D.T. designed research; J.D.T. performed research; J.D.T. analyzed data; and J.D.T. and D.C.C. wrote the paper.

The authors declare no competing interest.

This article is a PNAS Direct Submission.



[1]To whom correspondence may be addressed. Email: toner2@uw.edu.

This article contains supporting information online at https://www.pnas.org/lookup/suppl/doi:10.1073/pnas.1916109117/-/DCSupplemental.

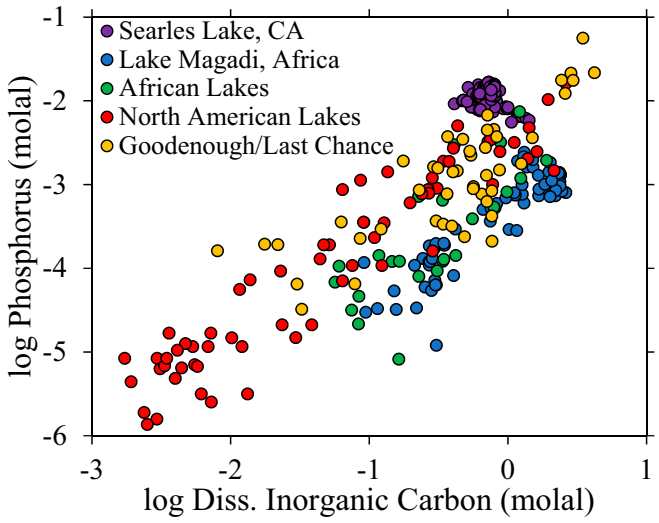


**Fig. 1.** Phosphorus concentrations in carbonate-rich lakes, including Searles Lake (19, 69), Lake Magadi (22, 23), Goodenough and Last Chance Lakes (20, 36), various other North American lakes (36, 69–71), and various other African lakes (72–75). Inorganic phosphate was determined in most analyses; however, the Goodenough and Last Chance Lake analyses are for total phosphorus (inorganic + organic).

periods of desiccation in the summer and autumn (20, 21). Other carbonate-rich lakes, such as Lake Magadi in Africa (22, 23) and Mono Lake in California (24), contain ~1 mM phosphate.

Closed-basin lakes accumulate high salt concentrations, including phosphates, from chemical weathering within their hydrologic basins, followed by the inflow of weathering products via streams to evaporating lake brines (25). Carbonate-rich lakes, in particular, develop when atmospheric or volcanogenic $CO_2$ gas dissolves in water to form carbonic acid ($H_2CO_3^0$), which chemically weathers rocks to form dissolved cations ($Na^+$, $K^+$, $Ca^{2+}$, and $Mg^{2+}$) and carbonate alkalinity ($CO_3^{2-}$ and $HCO_3^-$). Upon evaporation of these fluids, $Ca^{2+}$ and $Mg^{2+}$ ions precipitate as carbonates and silicates, and the residual carbonate alkalinity concentrates as Na–$HCO_3$–$CO_3$-rich brine (26).

Phosphate is thought to accumulate in carbonate-rich lakes because the carbonate alkalinity strongly precipitates $Ca^{2+}$ from solution as low-solubility $Ca^{2+}$ carbonates, which allows phosphate to reach much higher concentrations before saturating with respect to apatite (27, 28). However, the specific minerals that control $Ca^{2+}$ and phosphate concentrations, and the maximum phosphate concentrations possible, are unknown because apatites and carbonates form poorly defined and/or metastable phases in carbonate-rich brines. $Na^+$, $Mg^{2+}$, $CO_3^{2-}$, $SO_4^{2-}$, and $F^-$ ions typically found at high concentrations in carbonate-rich lakes extensively substitute in apatites (26, 29, 30), which greatly influences their solubility, nucleation, and crystallization rate (30). Furthermore, even low phosphate concentrations inhibit the nucleation and growth of both calcite ($CaCO_3$) and aragonite (a low-temperature $CaCO_3$ polymorph), so other carbonate phases likely control $Ca^{2+}$ concentrations in carbonate-rich lakes (31). A final issue is that biology cycles organic and inorganic phosphorus in carbonate-rich lakes, which makes it difficult to separate biotic vs. abiotic influences on phosphate concentrations.

## Experiments on Phosphate Accumulation in Carbonate-Rich Brines

The preceding considerations motivated a series of experiments to determine how much phosphate can accumulate by abiotic processes in carbonate-rich lakes. We start by noting that carbonate-rich lakes can only accumulate phosphate if $Ca^{2+}$ precipitates in carbonates instead of apatites; otherwise, phosphate will be removed from solution by much higher $Ca^{2+}$ influxes to lake basins. Consequently, how much phosphate can accumulate in carbonate-rich lakes is determined by what phases $Ca^{2+}$ preferentially precipitates in. If $Ca^{2+}$ precipitates as apatite, it will limit phosphate concentrations in the brine. On the other hand, if $Ca^{2+}$ carbonates form, then phosphate can accumulate at higher concentrations.

To investigate $Ca^{2+}$ precipitation in phosphate- and carbonate-rich brines, we slowly added $Ca^{2+}$ using gypsum ($CaSO_4 \cdot 2H_2O$) and phosphate using $Na_2HPO_4$ to various saturated $Na_2CO_3$/$NaHCO_3$ brines in the laboratory at room temperature (~23 °C). We then analyzed the salts that precipitated for mineralogy and chemistry (*Methods*). Results indicate that the formation of apatite and $Ca^{2+}$ carbonate salts depends primarily on the relative concentrations of carbonate ($CO_3^{2-}$) vs. bicarbonate ($HCO_3^-$) ions in solution (Fig. 2*A*). High $CO_3^{2-}$ ion concentrations strongly precipitate $Ca^{2+}$ from solution as gaylussite ($Na_2CO_3 \cdot CaCO_3 \cdot 5H_2O$) and/or calcite (open circles in Fig. 2*A*), which allows phosphate to accumulate up to ~100 mmol·kg$^{-1}$. Gaylussite is commonly found in carbonate-rich lakes, such as in Searles Lake and nearby Mono Lake (32); however, the formation of calcite is surprising because even trace phosphate levels inhibit calcite nucleation and growth (31). We infer that calcite probably formed indirectly through incongruent dissolution of primary gaylussite based on the slow conversion of gaylussite to calcite we observed over 4 wk (*SI Appendix*, *Appendix B*, Fig. S4), which is supported by observations of gaylussite converting into $CaCO_3$ in Mono Lake (33, 34).

At low $CO_3^{2-}$ ion concentrations, Na-rich carbonated apatites and calcite phases occur together, and phosphate concentrations in equilibrium with these minerals decrease with decreasing $CO_3^{2-}$ (black circles near the left of the vertical axis in Fig. 2*A*). These results are consistent with $Ca^{2+}$ from carbonate salts controlling the solubility of apatite. A decrease in $CO_3^{2-}$ ion concentration increases the solubility of calcite/gaylussite, which increases the concentration of $Ca^{2+}$ in solution and causes phosphate to precipitate as apatite.

The relative proportion of $CO_3^{2-}$ vs. $HCO_3^-$ ions in solution also controls the $pCO_2$ and pH, which we model for the experimental saturated Na–$HCO_3$–$CO_3$ brines in Fig. 2*B* (*SI Appendix*, *Appendix B*, Table S1 and *Methods*). By comparing modeled $pCO_2$ values to recent estimates ranging from 0.01 to 1 bar $CO_2$ on the early Earth (35), we find that corresponding phosphate concentrations in our experiments are between 20 and 100 mmol·kg$^{-1}$, respectively. Furthermore, the pH ranges from circumneutral at 1 bar $pCO_2$ to pH 9 at 0.01 bar $pCO_2$ in saturated Na–$HCO_3$–$CO_3$ brines because the relatively high $pCO_2$ acidifies the solutions. This suggests that elevated phosphate concentrations could have occurred in $CO_2$-rich atmospheres on the early Earth.

## Evaporative Concentration of Phosphate-Rich Brines

Our experiments indicate that when $Ca^{2+}$ is added to phosphate- and carbonate-rich brines, apatite minerals only precipitate above 10 to 100 mmol·kg$^{-1}$ phosphate. Applied to a closed-basin lake setting, this means that phosphate delivered via streams can accumulate up to ~100 mmol·kg$^{-1}$; however, at higher phosphate concentrations, $Ca^{2+}$ delivered by stream inflows will precipitate phosphate from solution as apatite. Given that streams have much more $Ca^{2+}$ than phosphate (36), closed-basin lakes in hydrologic balance (i.e., stream inflows balance water loss via evaporation) are constrained to <100 mmol·kg$^{-1}$ phosphate. However, once a phosphate-rich lake forms, the brine contains much more phosphate than $Ca^{2+}$ because $Ca^{2+}$ is sequestered into carbonate minerals (see *SI Appendix*, *Appendix A* for lake

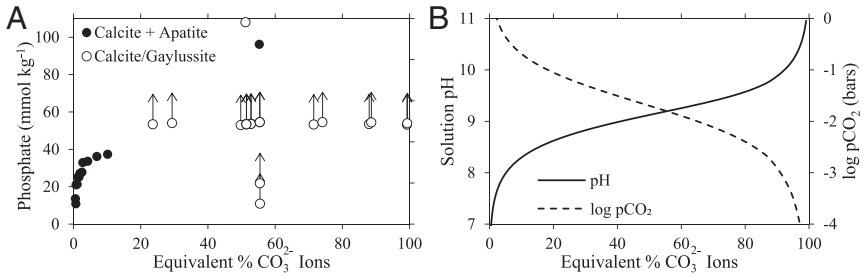


**Fig. 2.** Results from experiments on phosphate- and carbonate-rich brines. (*A*) The concentration of phosphate in saturated Na–$HCO_3$–$CO_3$ brines after 2 wk of equilibration with 50 to 100 mmol·kg$^{-1}$ $Ca^{2+}$ in the form of gypsum ($CaSO_4{\cdot}2H_2O$) and initial phosphate concentrations from 10 to 100 mmol·kg$^{-1}$. Solid circles indicate solutions saturated with respect to both apatite and calcite (determined via XRD; see *Methods*). Open circles indicate solutions that are saturated with respect to calcite and/or gaylussite ($Na_2CO_3{\cdot}CaCO_3{\cdot}5H_2O$); hence, phosphate must be more concentrated than these points for apatite to precipitate (indicated by the upwards arrows). The *x* axis gives the equivalent percentage of $CO_3^{2-}$ ions relative to the total carbonate alkalinity, that is, $100\times 2CO_3^{2-}/(2CO_3^{2-}+HCO_3^-)$. (*B*) The modeled $pCO_2$ and pH of the experimental saturated Na–$HCO_3$–$CO_3$ brines at 25 °C, which correspond to the solutions in *A*.

data). Consequently, in the absence of stream inflows, evaporating lake brines can reach much higher phosphate concentrations. Such evaporation may occur seasonally because of wet and dry cycles. Alternatively, lake brines may desiccate in shoreline environments by evaporation on rocks wetted by wave action or evaporation in local pools.

During lake evaporation (in the absence of Ca-rich stream inflows), phosphate will accumulate in the residual brine until it precipitates with a more concentrated cation as a salt. This phosphate-limiting salt cannot be a $Ca^{2+}$ or $Mg^{2+}$ phase because these ions are minor in carbonate-rich brines. We can also exclude $K^+$ because it is minor relative to $Na^+$ in carbonate-rich lakes and only precipitates phosphate salts at extremely high concentrations (37). The remaining major cation is $Na^+$, which implies that phosphate concentrations will increase in evaporating lake brines until the brine reaches saturation with respect to sodium phosphate salts. In addition, high phosphate concentrations would only form after sodium carbonate/bicarbonate and chloride salts had precipitated because phosphate is minor relative to both carbonate alkalinity and chloride.

To determine the maximum phosphate concentrations possible in such brines, we model solutions saturated with respect to sodium phosphate, carbonate, and chloride salts at variable temperature (0 to 50 °C) and $CO_2$ gas pressure (log $pCO_2$ −3.5 to 0 bars). We find that up to 3 molal phosphate occurs in equilibrium with either $Na_2HPO_4{\cdot}7H_2O$ or $Na_2HPO_4{\cdot}2H_2O$ salts (Fig. 3*A*). Relative to pure sodium phosphate solutions (Fig. 3*A*, red lines), phosphate concentrations in saturated mixed brines (Fig. 3*A*, black lines) decrease by about one-third because the additional $Na^+$ associated with chlorides and carbonates forces $Na_2HPO_4$ to precipitate from solution. The carbonate alkalinity precipitates as either nahcolite ($NaHCO_3$), natron ($Na_2CO_3{\cdot}10H_2O$), or trona ($Na_2CO_3{\cdot}NaHCO_3{\cdot}2H_2O$) depending on the $pCO_2$, and chloride ions precipitate as halite (NaCl).

The modeled pH of saturated phosphate brines depends on the temperature and atmospheric $pCO_2$ (Fig. 3*B*). At present-day $pCO_2$ levels, solutions are highly alkaline (pH ~ 10), consistent with high pHs measured in modern soda lakes (38); however, in $CO_2$-rich atmospheres on the early Earth (log $pCO_2$ = −2 to 0) brines range from moderately alkaline (pH 9) to slightly acidic (pH 6.5) because of acidification by $CO_2$. These are maximum pH values because the solutions are saturated with respect to carbonate alkalinity; hence, for undersaturated solutions the pH will be lower. Temperature also affects the pH because $CO_2$ is more soluble in solutions at lower temperatures. These results provide a plausible environmental scenario for molar phosphate concentrations at moderate pH levels used in prebiotic syntheses (8).

## Carbonate-Rich Lakes on the Early Earth

Carbonate-rich lakes may have been relatively common on early Earth due to strong chemical weathering of abundant, fresh volcanic rocks (39) under early Earth's $CO_2$-rich atmosphere (40). Weathering would release phosphate from apatites and carbonate alkalinity from other minerals, which would accumulate in closed basins (41, 42). A potential analog for such carbonate-rich

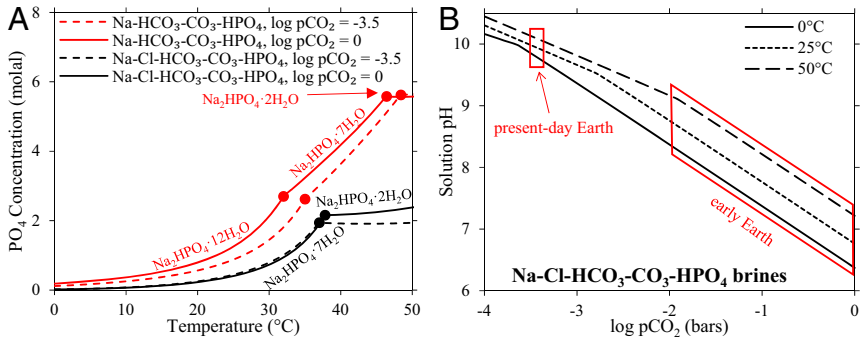


**Fig. 3.** Phosphate concentrations and pH modeled in saturated, carbonate-rich lake brines. (*A*) The concentration of phosphate in solutions saturated with respect to sodium phosphate. The red lines indicate the solubility of pure $Na_2HPO_4{\cdot}XH_2O$, where $XH_2O$ refers to the hydration state (X = 2, 7, and 12). The black lines indicate the solubility of sodium phosphate in solutions saturated with respect to sodium phosphate, chloride, and carbonate salts. Solid lines are for 1 bar atmospheric $pCO_2$, and dashed lines are for log $pCO_2$ = −3.5 bar (the $pCO_2$ of present-day Earth). (*B*) The pH of solutions saturated with respect to sodium phosphate, chloride, and carbonate salts at variable temperature and $pCO_2$. The range of pH and temperature of these solutions encompasses that of the black lines in *A*.

lakes on the early Earth is Lonar Lake in central India, a $NaHCO_3$-rich lake formed from an impact crater in basalt host rock (43). Lonar Lake also precipitates gaylussite and calcite salts (44), but phosphate concentrations are relatively low (~5 μM) because algal blooms consume the phosphate (45).

A consequence of early Earth's $CO_2$-rich atmosphere is that it would have enhanced the weathering of hydroxyl- and fluorapatites in mafic rocks by lowering the pH of surface waters (46, 47). Apatites are more soluble at lower pH and weather more rapidly in $CO_2$-acidified stream and rainwater, resulting in potentially high phosphate fluxes to carbonate-rich lakes on the early Earth. By modeling the equilibrium solubility of fluorapatite and hydroxyapatite in the presence of calcite buffer as a function of temperature and $CO_2$ pressure (Fig. 4 and *Methods*), we find that relatively low $CO_2$ pressures on present-day Earth (log $pCO_2$ = −3.5) limit phosphate to ≤1 μM, which is consistent with phosphate concentrations found in most present-day rivers and surface waters. However, in $CO_2$-rich atmospheres relevant to the early Earth ($pCO_2$ = 0.01 to 1 bar) (35, 40), modeled phosphate concentrations are 10 to 100 times higher, which implies a much higher phosphate weathering flux on the early Earth from streams into lakes.

Phosphate concentrations were likely higher in prebiotic, carbonate-rich lakes because microbial phosphate sinks were absent. Modern carbonate-rich lake environments are some of the most productive ecosystems on Earth in terms of biomass turnover because of high nutrient levels (38). As a result, phosphate measured in modern carbonate-rich lakes is probably a minimum because microbes consume the phosphate and eventually deposit it in organic matter. This may explain why Lake Magadi in Africa, a surface lake with high biomass turnover, has over 10 times lower phosphate concentrations than Searles Lake (which cannot support photosynthetic microbes because it is a groundwater brine), despite the much higher carbonate alkalinity found in Lake Magadi (Fig. 1). Consequently, in the absence of microbial consumption, carbonate-rich lakes on the prebiotic Earth may have hosted higher phosphate concentrations than typically occur today.

A potential sink for soluble phosphate on the early Earth is reduced soluble iron ($Fe^{2+}$), which precipitates with phosphate as the low-solubility mineral vivianite [$Fe_3(PO_4)_2{\cdot}8H_2O$]. However, $Fe^{2+}$ also precipitates as siderite ($FeCO_3$) in carbonate-rich brines, which limits $Fe^{2+}$ to low levels and increases the solubility of phosphate from vivianite, similar to solubility relations in the $CaCO_3$–apatite system shown in Fig. 2. Furthermore, siderite is less soluble than calcite, and unlike calcite, the nucleation and growth of siderite is not inhibited by phosphate. Although siderite crystallizes relatively slowly from solution at low temperatures (48), near-equilibrium conditions occur on a timescale of hours to days, which is fast relative to inflow and evaporation processes in closed-basin lakes. This implies that $Fe^{2+}$ concentrations in anoxic, phosphate- and carbonate-rich brines will be lower than $Ca^{2+}$, which suggests that $Ca^{2+}$, not $Fe^{2+}$, would have controlled phosphate concentrations in carbonate-rich lakes on the early Earth.

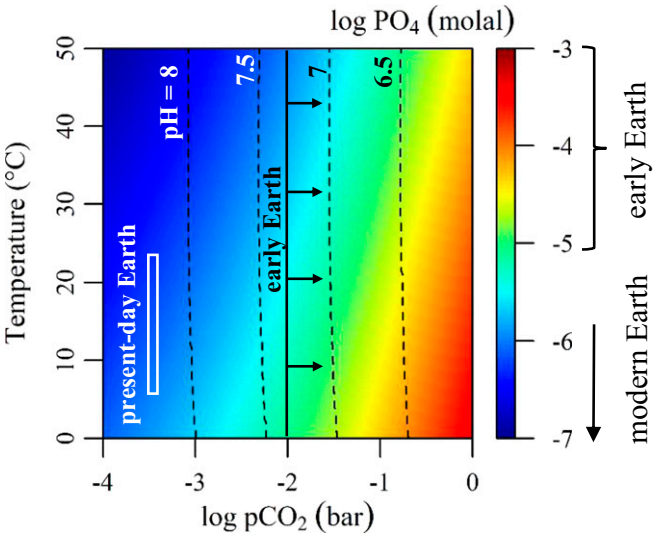


**Fig. 4.** Modeled phosphate concentrations (log $PO_4$) in equilibrium with fluorapatite, hydroxylapatite, and calcite at variable $pCO_2$ and temperature relevant to the release of phosphate into streams that supply lakes. The pH is given by dashed contours at 0.5-pH intervals.

## Implications for Prebiotic Chemistry

Our experiments and model results show that carbonate-rich lakes on the early Earth would have accumulated phosphate at concentration and pH levels relevant to laboratory prebiotic syntheses. Molar phosphate concentrations can occur during evaporation in lake marginal pools, on rocks wetted by wave action, and in shore sediments. Drying promotes condensation reactions such as phosphorylation by removing water (49), as well as more generally facilitating polymerization reactions (50). Condensation reactions may also have been promoted by deliquescence of highly soluble evaporites (51). Furthermore, carbonate-rich lakes are rich in clay, zeolite, and silica mineral assemblages that catalyze phosphorylation reactions because of their high reactive surface areas (52). Once phosphate reacts, changing lake levels or wave action could reintroduce the reaction products to the lake, or reaction products could undergo successive wet–dry cycles.

More broadly, closed-basin lakes are ideal sites for "one-pot" organic syntheses because they accumulate and concentrate reagents via evaporation across hydrologic basins (41, 49, 53). As a result, closed-basin lakes may have accumulated organic precursors for phosphorylation, as well as condensation agents that promote phosphorylation by forming reactive intermediate $PO_3^-$ species (54) and polyphosphates (14). Boron also accumulates at high concentrations in closed-basin lakes (e.g., Searles Lake contains ~0.5 molal boron; *SI Appendix, Appendix A*), which promotes the regioselective phosphorylation of ribose and stabilizes the furanose form needed to synthesize nucleic acids (55).

A difficulty for an origin of life in saline lakes is that high salt concentrations tend to destabilize lipid vesicles (56) and inhibit RNA oligimerization (57), but these issues are potentially resolvable. For example, lipid vesicles can stabilize in high-salt environments by binding to nucleotides and/or amino acids (58, 59). Given that concentrated prebiotic reagents and wet/dry cycles often used in the laboratory imply saline environments, more research is needed on prebiotic chemistry in salty solutions.

Recent attempts at "one-pot" syntheses have proposed closed-basin lakes as sites for the formation of amino acids, nucleotides, and lipid precursors in reaction networks involving ultraviolet light, phosphate, sulfur, and cyanide (53, 60). Our results indicate that high phosphate concentrations used in these reaction networks (8) plausibly occurred in carbonate-rich lake environments. Furthermore, the key cyanide component needed for this chemistry also preferentially accumulates in carbonate-rich lakes to make sodium ferrocyanide evaporites, which thermally decompose to sodium cyanide above 700 °C (possibly via magmatic activity or flash heating from asteroid impacts) (42, 53, 61). Concentrated sulfur needed for prebiotic syntheses may also have accumulated as sulfite ions (62). Consequently, carbonate-rich lakes accumulate a number of key reagents at high concentrations relevant to experimental prebiotic syntheses.

## Conclusions

The results presented here show that carbonate-rich lakes accumulate phosphate because $Ca^{2+}$ preferentially precipitates in gaylussite and/or calcite, which increases the solubility of apatites. In carbonate-rich lakes influenced by stream inflows, phosphate levels are limited to <0.1 molal because excess $Ca^{2+}$ in stream water precipitates apatite above this phosphate concentration threshold. However, in the absence of stream inflows, phosphate can enrich to >1 molal levels during evaporation because phosphate concentrations exceed $Ca^{2+}$ in carbonate-rich lakes. Such evaporation could occur continuously along lake margins, or during dry seasons.

Carbonate-rich lake environments were likely common on the early Earth due to chemical weathering of mafic rocks in early Earth's $CO_2$-rich atmosphere, and would have been relatively phosphate-rich compared to the present day because of efficient weathering of apatite minerals and the lack of microbial phosphate sinks. Furthermore, phosphate-rich brines on the early Earth would have had slightly acidic to moderately basic pH (pH 6.5 to 9) because of elevated atmospheric $CO_2$ levels. Thus, carbonate-rich lakes are highly plausible environments for accumulating phosphate at concentration and pH levels relevant to laboratory syntheses of prebiotic organophosphate compounds. Given the central importance of phosphate in cellular processes, and that phosphate occurs at micromolar concentrations elsewhere, our results specifically point to carbonate-rich lakes as sites for prebiotic chemistry and the origin of life.

## Methods

**Experimental $Ca^{2+}$ and Phosphate Precipitation in Carbonate-Rich Brines.** The goal of these experiments was to determine which salt phases precipitate $Ca^{2+}$ and phosphate ions in phosphate- and carbonate-rich brines. To achieve this, we added gypsum ($CaSO_4{\cdot}2H_2O$) to phosphate- and carbonate-rich brines prepared in the laboratory, and allowed the mixtures to react over 1 to 4 wk. The rationale behind this methodology is that the gypsum will slowly dissolve because it is sparingly soluble, gradually adding $Ca^{2+}$ to solution, which approximates the slow addition of $Ca^{2+}$ via inflow waters to closed-basin lakes. A potential complication to using gypsum as the $Ca^{2+}$ source is that gypsum will also add $SO_4^{2-}$ ions to solution; however, the added $SO_4^{2-}$ is <0.1 molal does not precipitate as a solid phase, and is not expected to interfere with the precipitation of carbonate or phosphate salts. After equilibration of the solution, we analyzed the resulting solid phases using inductively coupled optical emission spectroscopy (ICP-OES) and X-ray diffraction (XRD). The detailed results of these experiments are given in *SI Appendix, Appendix B*.

To prepare phosphate- and carbonate-rich brines, we gravimetrically added $NaHCO_3$, $Na_2CO_3$, $Na_2HPO_4$, and NaF reagents to 150 mL of deionized water in 250-mL polyethylene bottles. We added the $NaHCO_3$ and $Na_2CO_3$ reagents in varying proportions ranging from pure $NaHCO_3$ to pure $Na_2CO_3$ to make nearly saturated solutions (i.e., the concentration just below the point at which salt precipitates). We determined the saturation point for each Na–$HCO_3$–$CO_3$ mixture at 25 °C using the THEREDA Pitzer model described in *Geochemical Models*. We added the $Na_2HPO_4$ reagent at concentrations ranging from 10 to 500 mmol·kg$^{-1}$, and the NaF reagent at 0 and 10 mmol·kg$^{-1}$. Finally, we added $Ca^{2+}$ in the form of gypsum, capped the solutions, and agitated them with an orbital shaker for 1 to 4 wk.

We performed 4 series of experiments using the brine mixtures described above:

1) We varied the initial $NaHCO_3$:$Na_2CO_3$ ratio at constant equilibration time (2 wk) and initial phosphate concentration (50 mmol·kg$^{-1}$, the highest concentration measured in carbonate-rich lakes).
2) We varied the equilibration time at constant initial $NaHCO_3$:$Na_2CO_3$ ratio (0.6:0.4) and initial phosphate concentration (50 mmol·kg$^{-1}$).
3) We varied the initial phosphate concentration at constant equilibration time (2 wk) and initial $NaHCO_3$:$Na_2CO_3$ ratio (0.6:0.4).
4) We repeated experiments 1 and 3 described above with the addition of 10 mmol·kg$^{-1}$ $F^-$. These experiments are motivated by relatively high $F^-$ concentration commonly found in carbonate-rich lakes (*SI Appendix, Appendix B*), and because $F^-$ strongly precipitates with $Ca^{2+}$ and phosphate in natural systems to form fluorapatites.

**Analysis of Solids after Equilibration.** After the brine/salt mixtures equilibrated, we removed the solid phases by filtering. We then removed excess brine from the filtered solids by rinsing with ethanol and dried them in air for ~10 min. We then powdered the solid samples and analyzed them using a Bruker D8 Discover XRD from 10 to 60° 2θ. Furthermore, we analyzed the solids for Na, Ca, S, and P using ICP-OES. To prepare the solid samples for ICP-OES analysis, we first dried the samples in a vacuum oven at 60 °C overnight, and then acidified weighed aliquots of the dried samples (~50 mg) with 1 mL of ~2 M nitric acid (which completely dissolved the solid). The acid-dissolved samples were then diluted as needed for ICP-OES analysis.

We calculated the $CO_3^{2-}$ content of the equilibrated solid phases (on a dry weight basis) by assuming molar charge balance via the equation

$$[CO_3^{2-}] = [Ca^{2+}] + \frac{[Na^+]}{2} - \frac{3}{2}[PO_4^{3-}] - [SO_4^{2-}]. \quad [1]$$

The total calculated weight percent of $Ca^{2+}$, $Na^+$, $PO_4^{3-}$, $SO_4^{2-}$, and $CO_3^{2-}$ components on a dry basis is typically within several percentage of 100% (*SI Appendix, Appendix B*, Table S2).

**Calculation of Aqueous Species after Equilibration.** To calculate ion concentrations in the solutions after equilibration, we assumed that all of the $Ca^{2+}$ had completely precipitated as solid phases; consequently, the total concentration of all other ions precipitated from solution may be determined relative to $Ca^{2+}$. We also tested this assumption on a representative suite of samples and found that ~99.9% of the $Ca^{2+}$ remained in solid phases over the course of the experiments (see discussion in *SI Appendix, Appendix B*). For any given ion X, the concentration in solution after equilibration is given by

$$[X]_{\text{final solution}} = [X]_{\text{initial solution}} - [Ca^{2+}]_{\text{total}} \left( \frac{[X]}{[Ca^{2+}]} \right)_{\text{solid}}, \quad [2]$$

where subscripts indicate concentrations in the equilibrated solid, the initial, and the final solutions. We neglect $F^-$ concentrations because this ion is minor in the experimental solutions. Finally, to determine the pH, $pCO_2$, and inorganic carbon speciation of the equilibrated solutions, we modeled the solution composition determined above in equilibrium with 100 mL of headspace gas, which is the headspace volume in our experiments, using the THEREDA Pitzer model at 25 °C (described in *Geochemical Models*).

**Geochemical Models.** We use two approaches to model phosphate solubility at variable temperature and composition. To model solution chemistry at relatively low concentrations in Fig. 4, we use the phreeqc.dat database in the geochemical program PHREEQC (63). We supplemented phreeqc.dat with temperature-dependent equilibrium constants for fluorapatite [$Ca_5(PO_4)_3F$] (64) and hydroxylapatite [$Ca_5(PO_4)_3OH$] (65). To model concentrated solutions in the Na–Cl–P–$CO_2$–H–OH system from 0 to 60 °C in Fig. 3, we developed a Pitzer model in PHREEQC using parameters from several existing models. The resulting PHREEQC database file, as well as a detailed description of the Pitzer model equations and the model fits to literature data, are given in *SI Appendix, Appendix C*.

For Pitzer parameters involving NaCl, $NaHCO_3$, and $Na_2CO_3$ salts, we use Pitzer parameters and solubility products from CHEMCHAU (66), which is parameterized from 0 to 100 °C. We include NaCl, $Na_2CO_3{\cdot}7H_2O$, $Na_2CO_3{\cdot}H_2O$, $NaHCO_3$, $Na_2CO_3{\cdot}10H_2O$, $NaHCO_3{\cdot}Na_2CO_3{\cdot}2H_2O$, and $CO_2$ gas phases from CHEMCHAU. For phosphate Pitzer parameters, we use parameters from the THEREDA R-12 Pitzer database (37, 67, 68), and assume that Pitzer parameters involving phosphate are temperature-invariant. To model the temperature-dependent solubility of $Na_2HPO_4{\cdot}12H_2O$, $Na_2HPO_4{\cdot}7H_2O$, $Na_2HPO_4{\cdot}2H_2O$, $Na_2HPO_4$, $NaH_2PO_4{\cdot}2H_2O$, $NaH_2PO_4{\cdot}H_2O$, and $NaH_2PO_4$ solid phases, we fit literature data on the solubility of these salts to the temperature-dependent expression for equilibrium constants in PHREEQC, using the THEREDA solubility product at 25 °C as a basis. Finally, to model the dissociation constants of phosphoric acid ($H_3PO_4$) to $H_2PO_4^-$, $HPO_4^{2-}$, and $PO_4^{3-}$, we use the temperature-dependent dissociation constants in the phreeqc.dat database.

**Data Availability.** Experimental data from this study are available in *SI Appendix, Appendix B*, Tables S1 and S2. The PHREEQC database file used to make Fig. 3 is given in *SI Appendix, Appendix C*.

**ACKNOWLEDGMENTS.** We thank 2 anonymous reviewers for their constructive comments. This research was funded by the Simons Collaboration on the Origin of Life grant 511570 (to D.C.C.).

1. A. Gulick, Phosphorus as a factor in the origin of life. *Am. Sci.* **43**, 479–489 (1955).
2. M. A. Pasek, M. Gull, B. Herschy, Phosphorylation on the early Earth. *Chem. Geol.* **475**, 149–170 (2017).
3. M. A. Pasek, T. P. Kee, "On the origin of phosphorylated biomolecules" in *Origins of Life: The Primal Self-Organization*, R. Egal, D.-H. Lankenau, A. Y. Mulkidjanian, Eds. (Springer, Berlin, 2011), pp. 57–84.
4. A. W. Schwartz, Phosphorus in prebiotic chemistry. *Philos. Trans. R. Soc. Lond. B Biol. Sci.* **361**, 1743–1749, discussion 1749 (2006).
5. F. H. Westheimer, Why nature chose phosphates. *Science* **235**, 1173–1178 (1987).
6. W. L. Lindsay, *Chemical Equilibria in Soils* (John Wiley & Sons, New York, 1979).
7. C. Fernández-García, A. J. Coggins, M. W. Powner, A chemist's perspective on the role of phosphorus at the origins of life. *Life (Basel)* **7**, 1–23 (2017).
8. M. W. Powner, B. Gerland, J. D. Sutherland, Synthesis of activated pyrimidine ribonucleotides in prebiotically plausible conditions. *Nature* **459**, 239–242 (2009).
9. G. J. Handschuh, L. E. Orgel, Struvite and prebiotic phosphorylation. *Science* **179**, 483–484 (1973).
10. M. Gull, M. A. Pasek, Is struvite a prebiotic mineral? *Life (Basel)* **3**, 321–330 (2013).
11. C. Gibard, S. Bhowmik, M. Karki, E. K. Kim, R. Krishnamurthy, Phosphorylation, oligomerization and self-assembly in water under potential prebiotic conditions. *Nat. Chem.* **10**, 212–217 (2018).
12. R. Saladino, C. Crestini, S. Pino, G. Costanzo, E. Di Mauro, Formamide and the origin of life. *Phys. Life Rev.* **9**, 84–104 (2012).
13. B. Burcar *et al*., Darwin's warm little pond: A one-pot reaction for prebiotic phosphorylation and the mobilization of phosphate from minerals in a urea-based solvent. *Angew. Chem. Int. Ed. Engl.* **55**, 13249–13253 (2016).
14. A. D. Keefe, S. L. Miller, Potentially prebiotic syntheses of condensed phosphates. *Orig. Life Evol. Biosph.* **26**, 15–25 (1996).
15. M. Karki, C. Gibard, S. Bhowmik, R. Krishnamurthy, Nitrogenous derivatives of phosphorus and the origins of life: Plausible prebiotic phosphorylating agents in water. *Life (Basel)* **7**, 1–28 (2017).
16. M. A. Pasek, Rethinking early Earth phosphorus geochemistry. *Proc. Natl. Acad. Sci. U.S.A.* **105**, 853–858 (2008).
17. D. W. Deamer, *Assembling Life: How Can Life Begin on Earth and Other Habitable Planets?* (Oxford University Press, 2018).
18. A. Y. Mulkidjanian, A. Y. Bychkov, D. V. Dibrova, M. Y. Galperin, E. V. Koonin, Origin of first cells at terrestrial, anoxic geothermal fields. *Proc. Natl. Acad. Sci. U.S.A.* **109**, E821–E830 (2012).
19. G. I. Smith, M. Stuiver, Subsurface stratigraphy and geochemistry of late Quaternary evaporites, Searles Lake, California. *Geol. Surv. Prof. Pap.* **1043**, 1–130 (1979).
20. J. F. Hirst, "Sedimentology, diagenesis and hydrochemistry of the saline, alkaline lakes on the Cariboo Plateau, Interior British Columbia, Canada," PhD thesis, University of Saskatchewan, Saskatoon (2013).
21. R. W. Renaut, P. R. Long, Sedimentology of the saline lakes of the Cariboo plateau, Interior British Columbia, Canada. *Sediment. Geol.* **64**, 239–264 (1989).
22. H. P. Eugster, Chemistry and origin of the brines of Lake Magadi, Kenya. *Mineral. Soc. Am. Spec. Pap.* **3**, 213–235 (1970).
23. B. F. Jones, H. P. Eugster, S. L. Rettig, Hydrochemistry of the lake Magadi basin, Kenya. *Geochim. Cosmochim. Acta* **41**, 53–72 (1977).
24. Mono Basin Ecosystem Study Committee and National Research Council, "The Mono Basin ecosystem: Effects of changing lake level" (National Academies Press, Washington, DC, 1987), p. 272.
25. L. H. Hardie, H. P. Eugster, The evolution of closed-basin brines. *Mineral. Soc. Am. Spec. Pap.* **3**, 273–290 (1970).
26. H. P. Eugster, L. A. Hardie, "Saline lakes" in *Lakes* (Springer, New York, 1978), pp. 237–293.
27. R. A. Gulbrandsen, Physical and chemical factors in the formation of marine apatite. *Econ. Geol.* **64**, 365–382 (1969).
28. Y. Nathan, E. Sass, Stability relations of apatites and calcium carbonates. *Chem. Geol.* **34**, 103–111 (1981).
29. H. P. Eugster, B. F. Jones, Behavior of major solutes during closed-basin brine evolution. *Am. J. Sci.* **279**, 609–631 (1979).
30. D. McConnell, *Apatite: Its Crystal Chemistry, Mineralogy, Utilization, and Geologic and Biologic Occurrences* (Springer-Verlag, New York, 1973).
31. M. M. Reddy, Crystallization of calcium carbonate in the presence of trace concentrations of phosphorus-containing anions: I. Inhibition by phosphate and glycerophosphate ions at pH 8.8 and 25°C. *J. Cryst. Growth* **41**, 287–295 (1977).
32. J. J. Fahey, Saline minerals of the Green River formation. *U.S. Geol. Surv. Prof. Pap.* **405**, 1–50 (1962).
33. J. L. Bischoff, D. B. Herbst, R. J. Rosenbauer, Gaylussite formation at Mono Lake, California. *Geochim. Cosmochim. Acta* **55**, 1743–1747 (1991).
34. J. L. Bischoff, S. Stine, R. J. Rosenbauer, J. A. Fitzpatrick, T. W. Stafford, Jr, Ikaite precipitation by mixing of shoreline springs and lake water, Mono Lake, California, USA. *Geochim. Cosmochim. Acta* **57**, 3855–3865 (1993).
35. J. Krissansen-Totton, G. N. Arney, D. C. Catling, Constraining the climate and ocean pH of the early Earth with a geological carbon cycle model. *Proc. Natl. Acad. Sci. U.S.A.* **115**, 4105–4110 (2018).
36. F. W. Clarke, "The composition of the river and lake waters of the United States" (US Government Printing Office, 1924), p. 135.
37. T. Scharge, A. G. Muñoz, H. C. Moog, Thermodynamic modelling of high salinary phosphate solutions. I. Binary systems. *J. Chem. Thermodyn.* **64**, 249–256 (2013).
38. B. E. Jones, W. D. Grant, A. W. Duckworth, G. G. Owenson, Microbial diversity of soda lakes. *Extremophiles* **2**, 191–200 (1998).
39. K. C. Condie, *Earth as an Evolving Planetary System* (Academic Press, ed. 3, 2016).
40. K. Zahnle, L. Schaefer, B. Fegley, Earth's earliest atmospheres. *Cold Spring Harb. Perspect. Biol.* **2**, a004895 (2010).
41. E. E. Stüeken, R. Buick, A. J. Schauer, Nitrogen isotope evidence for alkaline lakes on late Archean continents. *Earth Planet. Sci. Lett.* **411**, 1–10 (2015).
42. J. D. Toner, D. C. Catling, Alkaline lake settings for concentrated prebiotic cyanide and the origin of life. *Geochim. Cosmochim. Acta* **260**, 124–132 (2019).
43. K. Fredriksson, A. Dube, D. J. Milton, M. S. Balasundaram, Lonar Lake, India: An impact crater in basalt. *Science* **180**, 862–864 (1973).
44. A. Anoop *et al*., Palaeoenvironmental implications of evaporative gaylussite crystals from Lonar Lake, central India. *J. Quaternary Sci.* **28**, 349–359 (2013).
45. D. H. Tambekar, A. L. Pawar, M. N. Dudhane, Lonar Lake water: Past and present. *Nat. Environ. Pollut. Technol.* **9**, 217–221 (2010).
46. J. Hao, D. A. Sverjensky, R. M. Hazen, Mobility of nutrients and trace metals during weathering in the late Archean. *Earth Planet. Sci. Lett.* **471**, 148–159 (2017).
47. P. M. Piccoli, P. A. Candela, Apatite in igneous systems. *Rev. Mineral. Geochem.* **48**, 255–292 (2002).
48. C. Jimenez-Lopez, C. S. Romanek, Precipitation kinetics and carbon isotope partitioning of inorganic siderite at 25°C and 1 atm. *Geochim. Cosmochim. Acta* **68**, 557–571 (2004).
49. E. E. Stüeken *et al*., Did life originate from a global chemical reactor? *Geobiology* **11**, 101–126 (2013).
50. D. S. Ross, D. Deamer, Dry/wet cycling and the thermodynamics and kinetics of prebiotic polymer synthesis. *Life (Basel)* **6**, 1–12 (2016).
51. T. D. Campbell *et al*., Prebiotic condensation through wet-dry cycling regulated by deliquescence. *Nat. Commun.* **10**, 4508 (2019).
52. R. M. Hazen, D. A. Sverjensky, Mineral surfaces, geochemical complexities, and the origins of life. *Cold Spring Harb. Perspect. Biol.* **2**, a002162 (2010).
53. B. H. Patel, C. Percivalle, D. J. Ritson, C. D. Duffy, J. D. Sutherland, Common origins of RNA, protein and lipid precursors in a cyanosulfidic protometabolism. *Nat. Chem.* **7**, 301–307 (2015).
54. R. Lohrmann, L. E. Orgel, Urea-inorganic phosphate mixtures as prebiotic phosphorylating agents. *Science* **171**, 490–494 (1971).
55. A. Ricardo, M. A. Carrigan, A. N. Olcott, S. A. Benner, Borate minerals stabilize ribose. *Science* **303**, 196 (2004).
56. D. Deamer, The role of lipid membranes in life's origin. *Life (Basel)* **7**, 1–17 (2017).
57. S. Miyakawa *et al*., Studies in the mineral and salt-catalyzed formation of RNA oligomers. *Orig. Life Evol. Biosph.* **36**, 343–361 (2006).
58. R. A. Black *et al*., Nucleobases bind to and stabilize aggregates of a prebiotic amphiphile, providing a viable mechanism for the emergence of protocells. *Proc. Natl. Acad. Sci. U.S.A.* **110**, 13272–13276 (2013).
59. C. E. Cornell *et al*., Prebiotic amino acids bind to and stabilize prebiotic fatty acid membranes. *Proc. Natl. Acad. Sci. U.S.A.* **116**, 17239–17244 (2019).
60. D. J. Ritson, C. Battilocchio, S. V. Ley, J. D. Sutherland, Mimicking the surface and prebiotic chemistry of early Earth using flow chemistry. *Nat. Commun.* **9**, 1821 (2018).
61. B. Burcar *et al*., A Stark contrast to modern Earth: Phosphate mineral transformation and nucleoside phosphorylation in an iron and cyanide-rich Early Earth scenario. *Angew. Chem. Int. Ed. Engl.* **58**, 16981–16987 (2019).
62. S. Ranjan, Z. R. Todd, J. D. Sutherland, D. D. Sasselov, Sulfidic anion concentrations on early earth for surficial origins-of-life chemistry. *Astrobiology* **18**, 1023–1040 (2018).
63. C. A. J. Appelo, D. Postma, *Geochemistry, Groundwater and Pollution* (CRC Press, Boca Raton, FL, ed. 2, 2005).
64. H. G. McCann, The solubility of fluorapatite and its relationship to that of calcium fluoride. *Arch. Oral Biol.* **13**, 987–1001 (1968).
65. H. McDowell, T. M. Gregory, W. E. Brown, Solubility of $Ca_5(PO_4)_3OH$ in the system $Ca(OH)_2$-$H_3PO_4$-$H_2O$ at 5, 15, 25, and 37°C. *J. Res. Natl. Bur. Stand., A Phys. Chem.* **81A**, 273–281 (1977).
66. G. M. Marion, D. C. Catling, J. K. Crowley, J. S. Kargel, Modeling hot spring chemistries with applications to martian silica formation. *Icarus* **212**, 629–642 (2011).
67. T. Scharge, "Thermodynamic database for phosphate" in *Thermodynamic Reference Database* (THEREDA, 2017), pp. 1–24.
68. T. Scharge, A. G. Munoz, H. C. Moog, Thermodynamic modeling of high salinary phosphate solutions II. Ternary and higher systems. *J. Chem. Thermodyn.* **80**, 172–183 (2015).
69. H. C. Whitehead, J. H. Feth, Recent chemical analyses of waters from several closed-basin lakes and their tributaries in the western United States. *Geol. Soc. Am. Bull.* **72**, 1421–1425 (1961).
70. I. S. Allison, R. S. Mason, *Sodium Salts of Lake County, Oregon*. (Oregon Department of Geology and Mineral Industries, 1947), **vol. 17**, pp. 1–12.
71. V. C. Newton, D. W. Baggs, *Geologic Evaluation of the Alkali Lake Disposal Site* (State of Oregon, Department of Geology and Mineral Industries, 1971).
72. P. J. Ashton, F. R. Schoeman, Limnological studies on the Pretoria Salt Pan, a hypersaline maar lake. *Hydrobiologia* **99**, 61–73 (1983).
73. J. F. Imhoff, H. G. Sahl, G. S. Soliman, H. G. Trüper, The Wadi Natrun: Chemical composition and microbial mass developments in alkaline brines of eutrophic desert lakes. *Geomicrobiol. J.* **1**, 219–234 (1979).
74. J. F. Talling, I. B. Talling, The chemical composition of African lake waters. *Int. Rev. Gesamten Hydrobiol. Hydrograph.* **50**, 421–463 (1965).
75. J. M. Melack, P. Kilham, Photosynthetic rates of phytoplankton in East African alkaline, saline lakes. *Limnol. Oceanogr.* **19**, 743–755 (1974).

PNAS
www.pnas.org

# Supplementary Information for

## A carbonate-rich lake solution to the phosphate problem of the origin of life

Jonathan D. Toner and David C. Catling

Jonathan D. Toner
Email: toner2@uw.edu

**This PDF file includes:**





www.pnas.org/cgi/doi/10.1073/pnas.1916109117

**Supplementary Material**

## Appendix A: The composition of carbonate-rich lakes

Carbonate-rich lakes accumulate a number of ions, in addition to phosphate, from their hydrologic basins, and concentrate these ions until they precipitate from solution as salts (1) (Fig. S1). Most ion concentrations in carbonate-rich lakes, with the exception of $Ca^{2+}$ and $Mg^{2+}$, increase linearly with phosphate in approximately 1:1 trends (Fig. S1). This indicates that phosphate in carbonate-rich lakes behaves as a conservative solute, that is, it does not precipitate during evaporation as a salt. This is in stark contrast to the situation in most surface waters on Earth, where phosphate has a highly non-conservative behavior and precipitates as apatite minerals.

The conservative behavior of phosphate is best appreciated in relation to $Br^-$, one of the most conservative ions in carbonate-rich lake brines because it forms highly soluble salts and does not significantly coprecipitate with other halides. In general, phosphate varies with $Br^-$ along a 1:1 trend (the dashed line in the $Br^-$ vs. phosphate plot in Fig. S1), which indicates that phosphate also behaves as a conservative ion. Other ions, such as $Cl^-$ and $Na^+$, are also highly conservative and show a similar trend with phosphate.

The highest concentration ions in carbonate-rich lakes are invariably $Na^+$ and $Cl^-$. Sodium ion concentrations reach up to ~9 molal, at which point $Na^+$ precipitates as highly soluble NaCl and $NaHCO_3/Na_2CO_3$ phases. Similarly, $Cl^-$ concentrations up to ~6 molal are possible before the $Cl^-$ precipitates as halite (NaCl). In modern carbonate-rich lakes, phosphate concentrations above ~1 $mmol \cdot kg^{-1}$ commonly occur in brines saturated with respect to NaCl and $NaHCO_3/Na_2CO_3$ salts. $K^+$ ions have a similar chemistry to $Na^+$, but on average the $K^+/Na^+$ ratio in carbonate-rich lakes is ~0.05, and the highest concentrations are ~1 molal. Lower $K^+$ relative to $Na^+$ is caused by several factors. First, $K^+$ salts such as arcanite ($K_2SO_4$) and sylvite (KCl) are less soluble than their $Na^+$ analogs. Second, $K^+$ ions undergo irreversible ion exchange fixation and precipitates in secondary silicate minerals (1).

Other ions that have appreciable concentrations in carbonate-rich brines are boron species and $SO_4^{2-}$. Boron concentrations are especially high in Searles Lake (~0.4 molal) (2), although Owens lake in California also attains high boron concentrations during evaporation (3). Boron concentrations are limited by highly soluble borax salts ($Na_2B_4O_7 \cdot 10H_2O$) (4). On present-day Earth, boron derives from weathering of boron-enriched continental crust (5). Although less land was likely present at life's origin than today, trace boron could have accumulated in significant concentrations via evaporative concentration in closed-basin lakes even on small amounts of land, such as ocean islands. Finally, $SO_4^{2-}$ reaches concentrations of ~1 molal before precipitating as $Na^+$ and $K^+$ salts such as mirabillite ($Na_2SO_4 \cdot 10H_2O$), arcanite, and thenardite ($Na_2SO_4$).

$Ca^{2+}$ and $Mg^{2+}$ ions generally have relatively low concentrations in carbonate-rich lakes, as expected based on high concentrations of carbonate ions. In some cases, $Ca^{2+}$ and $Mg^{2+}$ attain maximum concentrations of ~10 mM in carbonate-rich lakes; however, we question the accuracy of such high literature values. Almost all of the high $Ca^{2+}$ values in Fig. S1 corresponding to high phosphate concentrations are from a single study (6). This study measured $Ca^{2+}$ and $Mg^{2+}$ using

Inductively Coupled Optical Emission Spectroscopy (ICP-OES); however, ICP-OES suffers from matrix effects when measuring trace components in concentrated solutions, which may raise the apparent ion concentration. Given that Ref. (6) gives little information on the analytical procedure, and that the $Ca^{2+}$ and $Mg^{2+}$ values are anomalously high, these measurements are of questionable accuracy. Other anomalously high $Ca^{2+}$ values are from analyses done prior to ~1920, and so are also of questionable accuracy.

As an example of possible inaccuracies in literature $Ca^{2+}$ analyses, Owens Lake, California, was analyzed prior to ~1920 and found to have ~1 mM $Ca^{2+}$ (7). In comparison, a later study done by highly competent researchers measured 0.05-0.2 mM $Ca^{2+}$ (3), which decrease with increasing carbonate alkalinity during evaporation as expected. We may also compare environmental $Ca^{2+}$ concentrations with careful laboratory measurements of calcite solubility in $Na_2CO_3$ solutions (8), which indicate $Ca^{2+}$ concentrations between 0.01-0.1 mM $Ca^{2+}$ depending on the inorganic carbon concentration. Furthermore, we measured $Ca^{2+}$ concentrations in several of the experimental brines in this manuscript (see SI Appendix B), and found that concentrations are ~0.1 mM.

Carbonate-rich lakes are rich in many other ions such as $F^-$, $Li^+$, silica, and trace metals (9-11). In particular, silica and trace metals accumulate because of the formation of more soluble ion complexes in the presence of high pH and/or high concentrations of background ions. Silica accumulates at relatively high concentrations in carbonate-rich lakes because $H_3SiO_4^-$ and $H_2SiO_4^{2-}$ species form at high pH, instead of $H_4SiO_4^0$ species at low pH. Similarly, trace metals are relatively soluble in carbonate-rich lakes because they form complexes with concentrated $Cl^-$, $OH^-$, $HCO_3^-$, and $CO_3^{2-}$ ions.

Finally, we note that phosphorus may be present in inorganic and organic forms. In most analyses presented in Fig. S1, phosphate is measured using colorimetric methods, which is sensitive only to dissolved inorganic phosphate; however, measurements of the bulk P content by atomic emission methods yields only the total dissolved P (inorganic + organic phosphorus). In these cases (e.g., the P analyses for Goodenough and Last Chance lakes), a fraction of the total measured dissolved P may be due to the dissolved organic phosphorus.

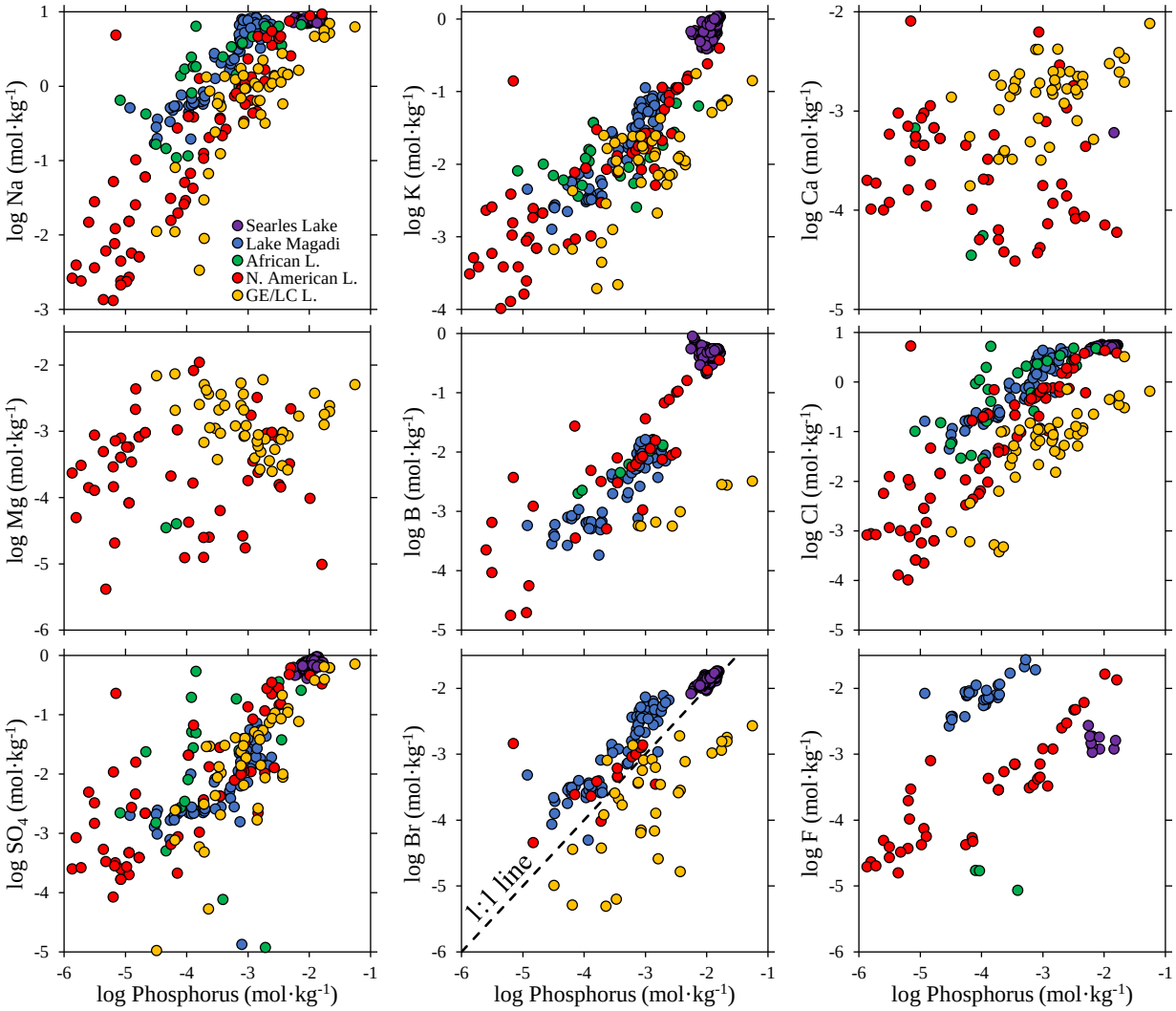


Fig. S1. Concentrations of P, $Na^+$, $K^+$, $Ca^{2+}$, $Mg^{2+}$, B, $Cl^-$, $SO_4^{2-}$, $Br^-$, and $F^-$ in Searles Lake, Lake Magadi, Goodenough and Last Chance lakes (GE/LC L.), various other African lakes (African L.), and various other North American Lakes (N. American L.). We only plot lake compositions that have been analyzed for phosphate/phosphorus. The dashed line in the $Br^-$ vs. phosphorus plot indicates the 1:1 trend expected for conservative solutes.

**Appendix B: Results of experiments on gypsum addition to phosphate-rich brines**

The results of our experiments on phosphate- and carbonate-rich brines in the lab are presented here. Table S1 describes the initial salt content of the solutions, the salt concentration after equilibration (calculated by accounting for ions precipitated in solid phases, as described in the *Methods* section), and the modeled pH, $pCO_2$, and $\%HCO_3$ in the equilibrated solution. Table S2 describes the composition of solid phases on a dry weight basis after equilibration, where the $CO_3^{2-}$ content is calculated based on charge balance (as described in the *Methods* section). Finally, the XRD profiles of the solid phases listed in Table S2 are presented in Fig. S2 through Fig. S6.

To check our modeled pH values listed in Table S1, we also measured the pH of several solutions with a standard glass electrode, and found that the measured pH was typically within 0.2 of the modeled value. We note that pH measurements in salt solutions are complicated by several sources of error, such as theoretical uncertainties on the value of single ion activity coefficients in concentrated solutions and liquid junction potential errors (12). Another possible issue is that the modeled pH is sensitive to errors in the composition of the precipitated salts, which we subtract from the initial prepared solution composition to arrive at the final solution composition. First, measured ion concentrations have likely errors of approximately ±5 % based on the accuracy of ICP-OES analyses. Second, errors in the assumed ionic speciation of the solid phases can affect the modeled pH. For precipitated solids, we assumed that only $CO_3^{2-}$ and $PO_4^{3-}$ ions were present, based on solids identified via XRD, but $HCO_3^-$ and $HPO_4^{2-}$ ions may also have been present in the solids. Removing $CO_3^{2-}$ and $PO_4^{3-}$ ions from the initial solution results in a lower modeled pH than if $HCO_3^-$ and $HPO_4^{2-}$ ions are removed. This is because $CO_3^{2-}$ and $PO_4^{3-}$ ions have more alkalinity than equivalent concentrations of $HCO_3^-$ and $HPO_4^{2-}$ ions.

Another key assumption in our analysis is that all of the $Ca^{2+}$ in the experimental solutions remained in solid phases. We tested this by measuring $Ca^{2+}$ in a representative suite of four samples using ICP-OES (sample numbers 1, 8, 9, and 11 in Table S1). To achieve the highest possible accuracy, we corrected for matrix effects by spiking each sample with known amounts of $Ca^{2+}$, and ensuring that no precipitates formed by acidifying with $HNO_3$. Each sample was analyzed with no added $Ca^{2+}$, followed by three replicate samples with increasing amounts of $Ca^{2+}$. We then calculate the $Ca^{2+}$ in the unspiked samples by linear regression of the spiked samples. The lowest concentration of $Ca^{2+}$ that we spiked the samples with was 0.1 $mmol \cdot kg^{-1}$. Our results indicate that $Ca^{2+}$ concentrations are 0.07, 0.11, 0.045, and 0.033 $mmol \cdot kg^{-1}$ for sample numbers 1, 8, 9, and 11 respectively in Table S1. For an initial added $Ca^{2+}$ concentration of 100 $mmol \cdot kg^{-1}$, this means that ~99.9 % of the added $Ca^{2+}$ remained in solid phases over the course of the experiment.

Table S1. The concentration of ions (molal) in the initial and final solutions equilibrated over 1 to 4 weeks. The initial total molality is the molality of all salts initially added to the experiment, including gypsum. The final aqueous molality is the solution molality after equilibration, which is calculated by assuming all $Ca^{2+}$ is present in solid phases, and subtracting ions precipitated in solid phases (see Table S2) from the initial total molality. Finally, the modeled values for the equilibrated solution were determined by modeling gas-solution equilibrium with 100 ml of headspace (as in the experimental set-up) using the geochemical program PHREEQC and the aqueous database THEREDA.

| | | Initial Total Molality | | | | | | Final Aqueous Molality | | | | | Modeled Aqueous Values | | |
|---|---|---|---|---|---|---|---|---|---|---|---|---|---|---|---|
| # | Time | Na | Ca | $SO_4$ | C | P | F | Na | $SO_4$ | C | P | F | pH | $\log_{10}(pCO_2)$ | $\%HCO_3$ |
| | weeks | | | | | | molal | | | | | | | bars | |
| | *Series 1: Variable $HCO_3$:$CO_3$ ratio, with and without fluoride* | | | | | | | | | | | | | | |
| 1 | 2 | 1.19 | 0.099 | 0.099 | 1.09 | 0.049 | | 1.17 | 0.099 | 1.04 | 0.014 | | 7.03 | 0.48 | 99.4 |
| 2 | 2 | 1.2 | 0.099 | 0.099 | 1.09 | 0.049 | | 1.19 | 0.099 | 1.04 | 0.011 | | 7.11 | 0.41 | 99.3 |
| 3 | 2 | 1.21 | 0.099 | 0.099 | 1.09 | 0.049 | | 1.2 | 0.099 | 1.03 | 0.021 | | 7.16 | 0.36 | 99.2 |
| 4 | 2 | 1.23 | 0.099 | 0.099 | 1.09 | 0.049 | | 1.23 | 0.099 | 1.03 | 0.021 | | 7.3 | 0.22 | 98.9 |
| 5 | 2 | 1.26 | 0.099 | 0.099 | 1.09 | 0.049 | | 1.25 | 0.099 | 1.03 | 0.025 | | 7.49 | 0.04 | 98.3 |
| 6 | 2 | 1.28 | 0.099 | 0.099 | 1.09 | 0.049 | | 1.27 | 0.099 | 1.01 | 0.033 | | 7.71 | -0.19 | 97.2 |
| 7 | 2 | 1.65 | 0.099 | 0.099 | 1.29 | 0.049 | | 1.64 | 0.099 | 1.19 | 0.049 | | 8.67 | -1.17 | 76.4 |
| 8 | 2 | 2.32 | 0.099 | 0.099 | 1.59 | 0.049 | | 2.26 | 0.099 | 1.46 | 0.048 | | 9.11 | -1.72 | 48.6 |
| 9 | 2 | 3.43 | 0.099 | 0.099 | 2.08 | 0.049 | | 3.23 | 0.099 | 1.88 | 0.048 | | 9.39 | -2.13 | 28.5 |
| 10 | 2 | 5.46 | 0.099 | 0.099 | 2.98 | 0.049 | | 5.31 | 0.099 | 2.81 | 0.049 | | 9.78 | -2.73 | 12 |
| 11 | 2 | 5.06 | 0.099 | 0.099 | 2.48 | 0.049 | | 4.91 | 0.099 | 2.31 | 0.048 | | 11.05 | -5.25 | 0.8 |
| 12 | 2 | 1.04 | 0.05 | 0.05 | 0.93 | 0.05 | 0.009 | 1.03 | 0.05 | 0.92 | 0.025 | 0.009 | 7.44 | 0.05 | 98.6 |
| 13 | 2 | 1.21 | 0.05 | 0.05 | 1.1 | 0.05 | 0.009 | 1.21 | 0.05 | 1.08 | 0.027 | 0.009 | 7.56 | 0 | 98.1 |
| 14 | 2 | 1.23 | 0.05 | 0.05 | 1.1 | 0.05 | 0.009 | 1.22 | 0.05 | 1.08 | 0.028 | 0.009 | 7.68 | -0.12 | 97.5 |
| 15 | 2 | 1.25 | 0.05 | 0.05 | 1.1 | 0.05 | 0.009 | 1.24 | 0.05 | 1.07 | 0.034 | 0.009 | 7.9 | -0.35 | 95.8 |
| 16 | 2 | 1.27 | 0.05 | 0.05 | 1.1 | 0.05 | 0.009 | 1.27 | 0.05 | 1.06 | 0.036 | 0.009 | 8.13 | -0.59 | 93 |
| 17 | 2 | 1.29 | 0.05 | 0.05 | 1.1 | 0.05 | 0.009 | 1.29 | 0.05 | 1.06 | 0.037 | 0.009 | 8.3 | -0.78 | 89.8 |
| 18 | 2 | 1.43 | 0.05 | 0.05 | 1.1 | 0.05 | 0.009 | 1.43 | 0.05 | 1.05 | 0.049 | 0.009 | 8.83 | -1.4 | 70.7 |
| 19 | 2 | 2.01 | 0.05 | 0.05 | 1.36 | 0.05 | 0.009 | 2 | 0.05 | 1.3 | 0.049 | 0.009 | 9.21 | -1.89 | 44.6 |
| 20 | 2 | 2.95 | 0.05 | 0.05 | 1.78 | 0.05 | 0.009 | 2.92 | 0.05 | 1.71 | 0.05 | 0.009 | 9.48 | -2.29 | 25.9 |
| 21 | 2 | 4.68 | 0.05 | 0.05 | 2.54 | 0.05 | 0.009 | 4.64 | 0.05 | 2.47 | 0.049 | 0.009 | 9.83 | -2.85 | 11.4 |
| 22 | 2 | 4.34 | 0.05 | 0.05 | 2.12 | 0.05 | 0.009 | 4.28 | 0.05 | 2.04 | 0.049 | 0.009 | 11.13 | -5.45 | 0.7 |
| | *Series 2: Variable equilibration time, without fluoride* | | | | | | | | | | | | | | |
| 23 | 1 | 2.33 | 0.099 | 0.099 | 1.59 | 0.049 | | 2.2 | 0.099 | 1.43 | 0.048 | | 9.09 | -1.69 | 50.3 |
| 24 | 2 | 2.33 | 0.1 | 0.1 | 1.59 | 0.05 | | 2.27 | 0.099 | 1.47 | 0.049 | | 9.11 | -1.72 | 48.6 |
| 25 | 3 | 2.32 | 0.099 | 0.099 | 1.59 | 0.049 | | 2.32 | 0.099 | 1.49 | 0.049 | | 9.13 | -1.74 | 47.2 |
| 26 | 4 | 2.32 | 0.099 | 0.099 | 1.59 | 0.049 | | 2.32 | 0.099 | 1.49 | 0.049 | | 9.13 | -1.74 | 47.2 |
| | *Series 3: Variable initial phosphate concentration, with and without fluoride* | | | | | | | | | | | | | | |
| 27 | 2 | 2.07 | 0.099 | 0.099 | 1.34 | 0.099 | | 2.06 | 0.099 | 1.24 | 0.098 | | 9.13 | -1.8 | 48.8 |
| 28 | 2 | 2.26 | 0.099 | 0.099 | 1.34 | 0.199 | | 2.2 | 0.099 | 1.28 | 0.148 | | 9.08 | -1.73 | 50.7 |
| 29 | 2 | 2.46 | 0.099 | 0.099 | 1.34 | 0.298 | | 2.39 | 0.099 | 1.29 | 0.243 | | 9.05 | -1.71 | 50.9 |
| 30 | 2 | 2.66 | 0.099 | 0.099 | 1.34 | 0.397 | | 2.59 | 0.099 | 1.29 | 0.339 | | 9.03 | -1.7 | 51 |
| 31 | 2 | 2.86 | 0.099 | 0.099 | 1.34 | 0.497 | | 2.8 | 0.099 | 1.3 | 0.436 | | 9.01 | -1.68 | 50.9 |
| 32 | 2 | 1.93 | 0.05 | 0.05 | 1.36 | 0.01 | 0.009 | 1.92 | 0.05 | 1.3 | 0.01 | 0.009 | 9.22 | -1.9 | 44.5 |
| 33 | 2 | 1.95 | 0.05 | 0.05 | 1.36 | 0.02 | 0.009 | 1.94 | 0.05 | 1.3 | 0.02 | 0.009 | 9.22 | -1.9 | 44.5 |
| 34 | 2 | 2.01 | 0.05 | 0.05 | 1.36 | 0.05 | 0.009 | 2 | 0.05 | 1.3 | 0.05 | 0.009 | 9.21 | -1.89 | 44.6 |
| 35 | 2 | 2.1 | 0.05 | 0.05 | 1.36 | 0.099 | 0.009 | 2.1 | 0.05 | 1.31 | 0.096 | 0.009 | 9.2 | -1.88 | 44.7 |
| 36 | 2 | 2.3 | 0.05 | 0.05 | 1.36 | 0.198 | 0.009 | 2.29 | 0.05 | 1.33 | 0.182 | 0.009 | 9.16 | -1.85 | 45.1 |

Table S2. The concentration of ions (wt. %) in solid phases after equilibration of the solutions given in Table S1, and drying at 60°C in a vacuum oven overnight. Na, Ca, P, and S were measured using inductively coupled optical emission spectroscopy (ICP-OES), whereas the $CO_3^{2-}$ content was calculated via charge balance (see Methods). Phases determined via XRD analysis (presented in Fig. S2 through Fig. S6) are given in the last column.

| # | Na | Ca | $PO_4$ | $SO_4$ | $CO_3$ | Total | XRD Phases |
|---|---|---|---|---|---|---|---|
| | | | wt. % | | | | |
| | *Series 1: Variable $HCO_3$:$CO_3$ ratio, with and without fluoride* | | | | | | |
| 1 | 3.46 | 33.34 | 28.66 | 0.77 | 26.88 | 93.12 | calcite, apatite |
| 2 | 2.52 | 37.7 | 34.88 | 0.06 | 26.75 | 101.91 | calcite, apatite |
| 3 | 1.81 | 38.12 | 26.02 | 0.46 | 34.59 | 101 | calcite, apatite |
| 4 | 2.08 | 37.47 | 25.31 | 0.3 | 34.75 | 99.91 | calcite, apatite |
| 5 | 1.82 | 36.93 | 21.42 | 0.22 | 37.34 | 97.73 | calcite, apatite |
| 6 | 1.37 | 37.99 | 15.08 | 0.25 | 44.33 | 99.01 | calcite, apatite |
| 7 | 0.79 | 39.09 | 0.85 | 0.13 | 58.78 | 99.65 | calcite |
| 8 | 9.68 | 27.25 | 0.62 | 0.14 | 52.83 | 90.53 | calcite, gaylussite |
| 9 | 20.25 | 17.07 | 0.42 | 0.15 | 51.53 | 89.41 | calcite, gaylussite |
| 10 | 18.26 | 20.95 | 0.42 | 0.34 | 54.64 | 94.61 | calcite, gaylussite |
| 11 | 18.47 | 20.63 | 0.54 | 0.4 | 54.28 | 94.31 | calcite, gaylussite |
| 12 | 2.61 | 36.98 | 43.1 | 0 | 18.03 | 100.72 | apatite |
| 13 | 2.91 | 35.84 | 38.6 | 0.09 | 20.93 | 98.36 | calcite, apatite |
| 14 | 2.84 | 36.9 | 38.56 | 0.1 | 22.45 | 100.86 | calcite, apatite |
| 15 | 2.75 | 37.31 | 28.55 | 0.2 | 32.37 | 101.17 | calcite, apatite |
| 16 | 2.18 | 38.47 | 24.8 | 0.1 | 36.99 | 102.53 | calcite, apatite |
| 17 | 2.12 | 38.03 | 22.32 | 0 | 38.67 | 101.14 | calcite, apatite |
| 18 | 0.53 | 39.68 | 0.98 | 0 | 59.29 | 100.49 | calcite |
| 19 | 0.65 | 39.98 | 0.21 | 0 | 60.62 | 101.45 | calcite |
| 20 | 12.07 | 27.46 | 0.08 | 0 | 56.86 | 96.47 | calcite, gaylussite |
| 21 | 14.33 | 26.47 | 0.21 | 0.1 | 58.14 | 99.25 | calcite, gaylussite |
| 22 | 17.8 | 23.06 | 0.68 | 0.09 | 57.12 | 98.75 | calcite, gaylussite |
| | *Series 2: Variable equilibration time, without fluoride* | | | | | | |
| 23 | 16.37 | 22.17 | 0.7 | 0.2 | 53.83 | 93.28 | calcite, gaylussite |
| 24 | 9.68 | 27.25 | 0.62 | 0.14 | 52.83 | 90.53 | calcite, gaylussite |
| 25 | 1.06 | 39.52 | 0.57 | 0.08 | 60.08 | 101.31 | calcite |
| 26 | 0.96 | 38.82 | 0.69 | 0.08 | 58.78 | 99.33 | calcite |
| | *Series 3: Variable initial phosphate concentration, with and without fluoride* | | | | | | |
| 27 | 1.13 | 38.57 | 1.07 | 0.11 | 58.25 | 99.13 | Ca-Na phosphate |
| 28 | 10.13 | 27.13 | 33.02 | 0.32 | 22.42 | 93.02 | Ca-Na phosphate |
| 29 | 10.99 | 27.63 | 36.33 | 0.41 | 21.09 | 96.45 | Ca-Na phosphate |
| 30 | 11.02 | 27.11 | 37.84 | 0.58 | 18.82 | 95.37 | Ca-Na phosphate |
| 31 | 10.31 | 28.04 | 40.47 | 0.5 | 16.85 | 96.16 | calcite |
| 32 | 0.57 | 40.05 | 0.03 | 0 | 60.79 | 101.43 | calcite, apatite |
| 33 | 0.55 | 38.83 | 0.06 | 0 | 58.91 | 98.35 | calcite, apatite |
| 34 | 0.58 | 40.19 | 0.18 | 0 | 60.88 | 101.82 | calcite |
| 35 | 1.07 | 38.79 | 5.68 | 0 | 54.2 | 99.73 | calcite |
| 36 | 3.62 | 35.89 | 28.86 | 0 | 31.21 | 99.58 | calcite |

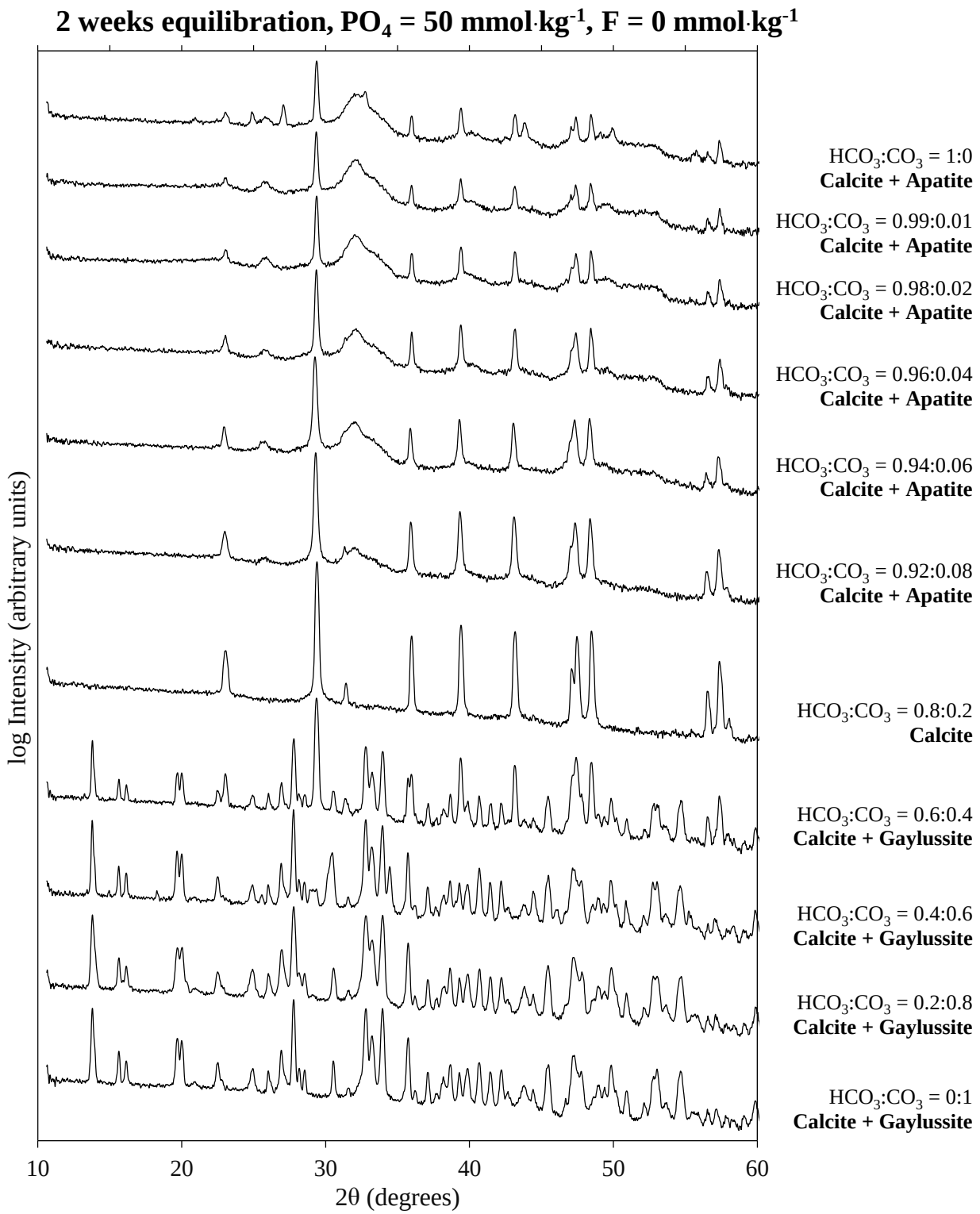


Fig. S2. XRD profiles of saturated carbonate brines containing 50 mmol·kg$^{-1}$ phosphate (no added $F^-$) equilibrated for two weeks at various $HCO_3$:$CO_3$ ratios. This corresponds to sample numbers 1 to 11 in Table S1 and Table S2.

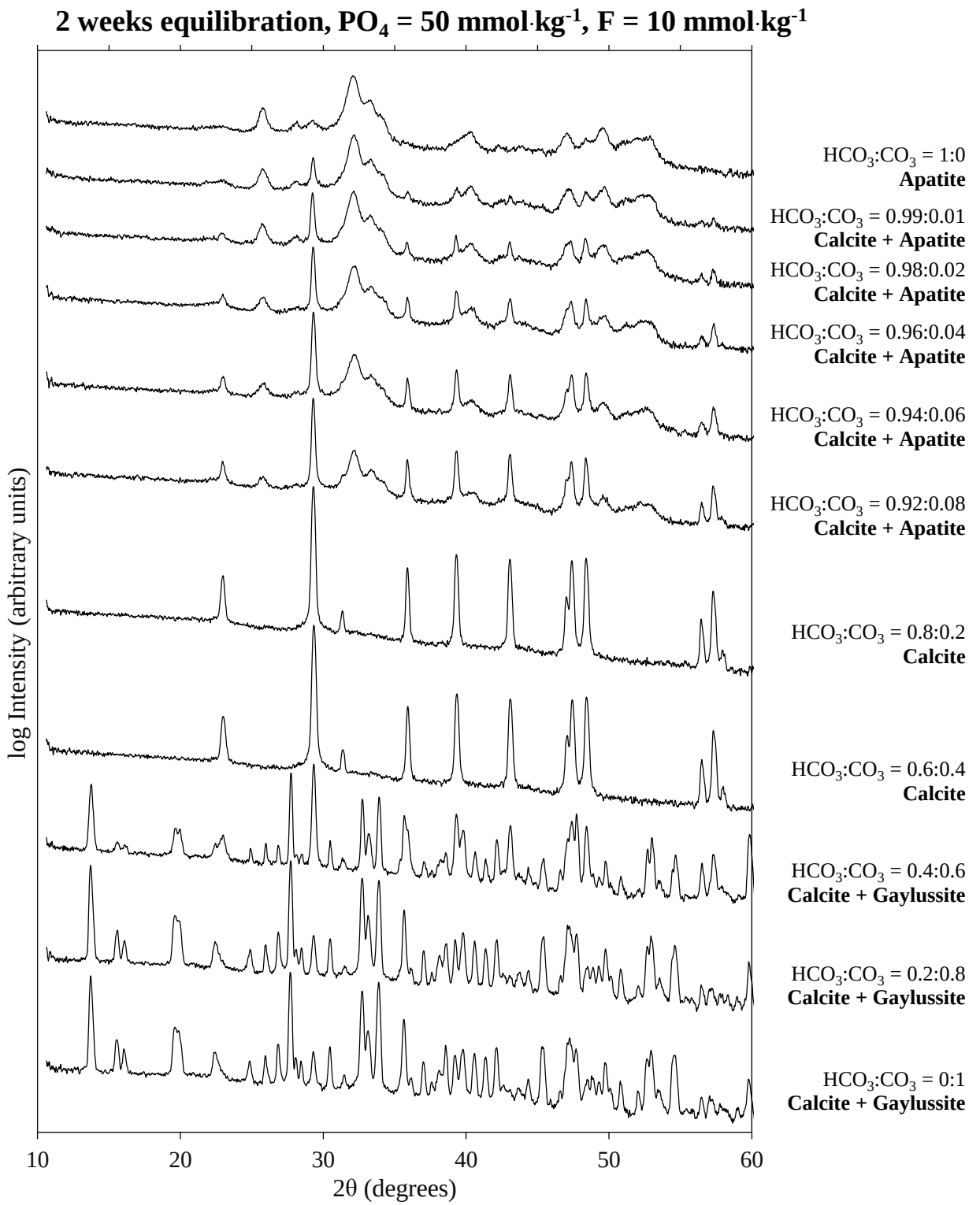


Fig. S3. XRD profiles of saturated carbonate brines containing 50 mmol·kg$^{-1}$ phosphate and 10 mmol·kg$^{-1}$ $F^-$ equilibrated for two weeks at various molar $HCO_3$:$CO_3$ ratios. This corresponds to sample numbers 12 to 22 in Table S1 and Table S2.

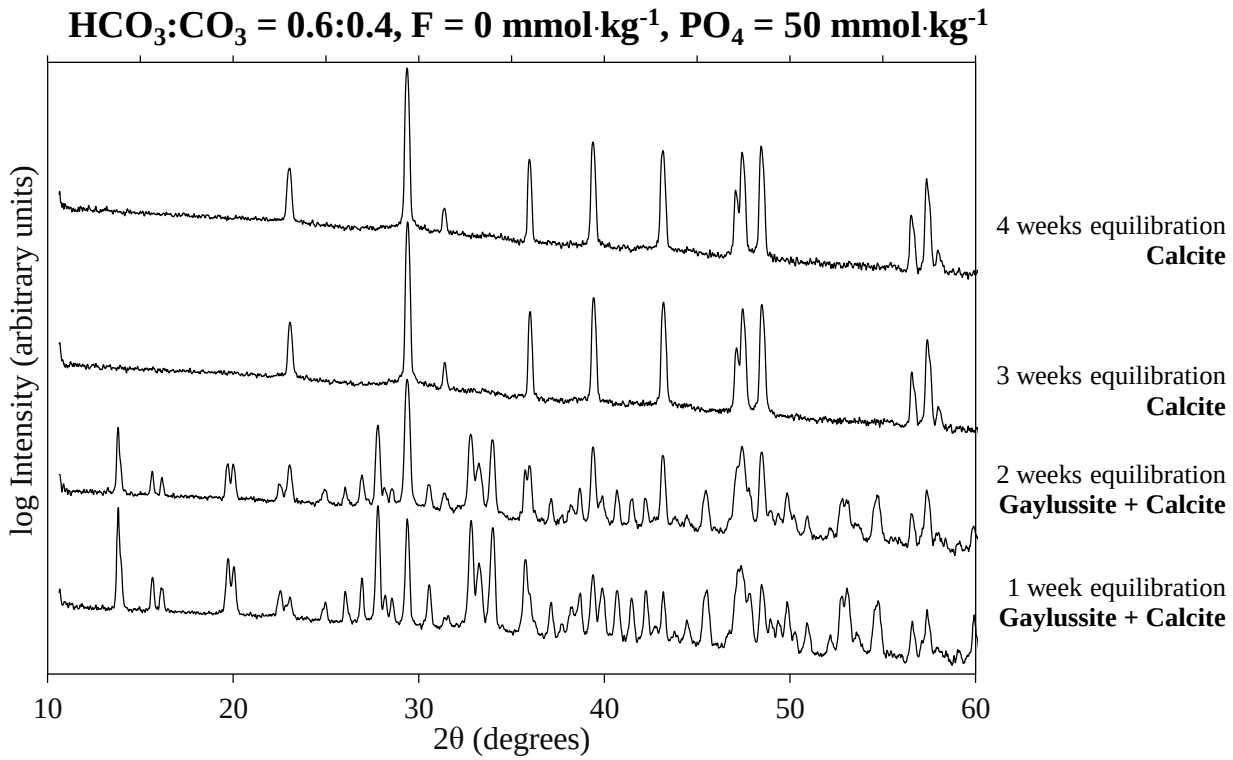


Fig. S4. XRD profiles of saturated carbonate brines with a molar $HCO_3$:$CO_3$ ratio of 0.6:0.4 (no added $F^-$) and an initial phosphate concentration of 50 mmol·kg$^{-1}$ equilibrated over one to four weeks. This corresponds to sample numbers 23 to 26 in Table S1 and Table S2.

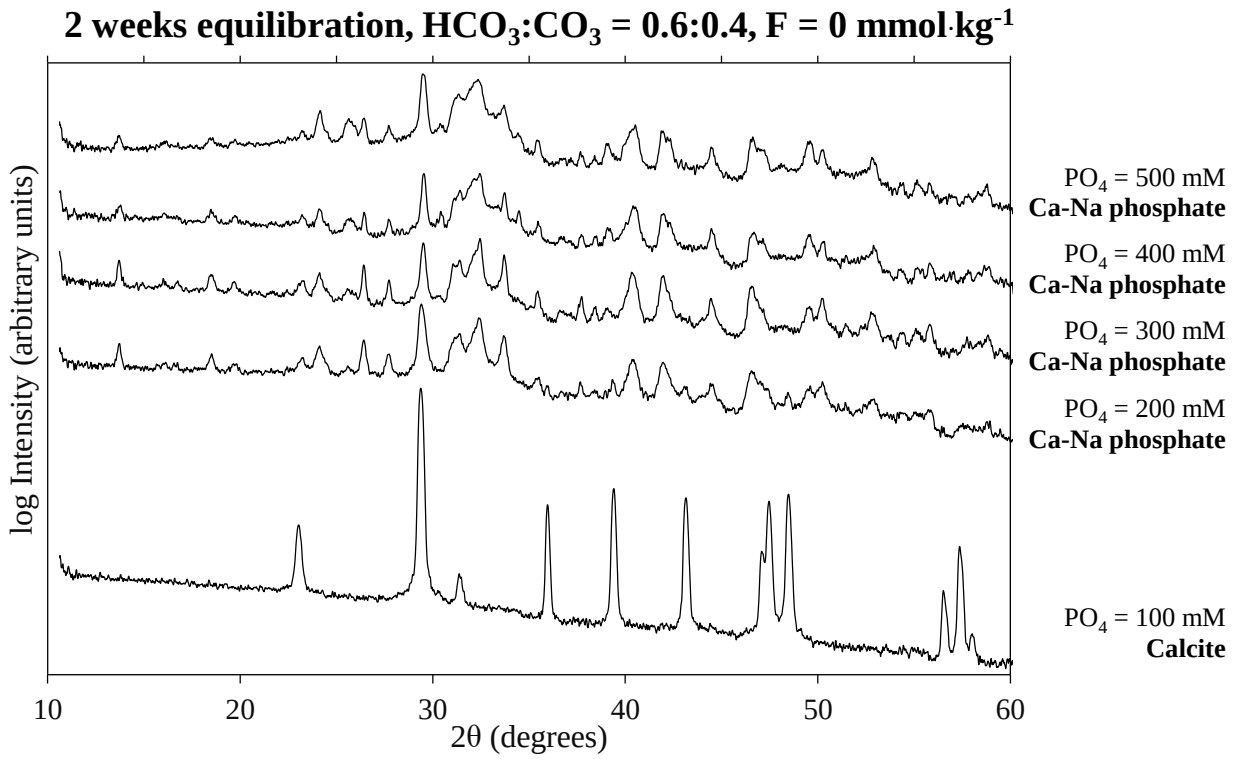


Fig. S5. XRD profiles of saturated carbonate brines with a molar $HCO_3$:$CO_3$ ratio of 0.6:0.4 (no added $F^-$) equilibrated for two weeks at various initial phosphate concentrations. This corresponds to sample numbers 27 to 31 in Table S1 and Table S2.

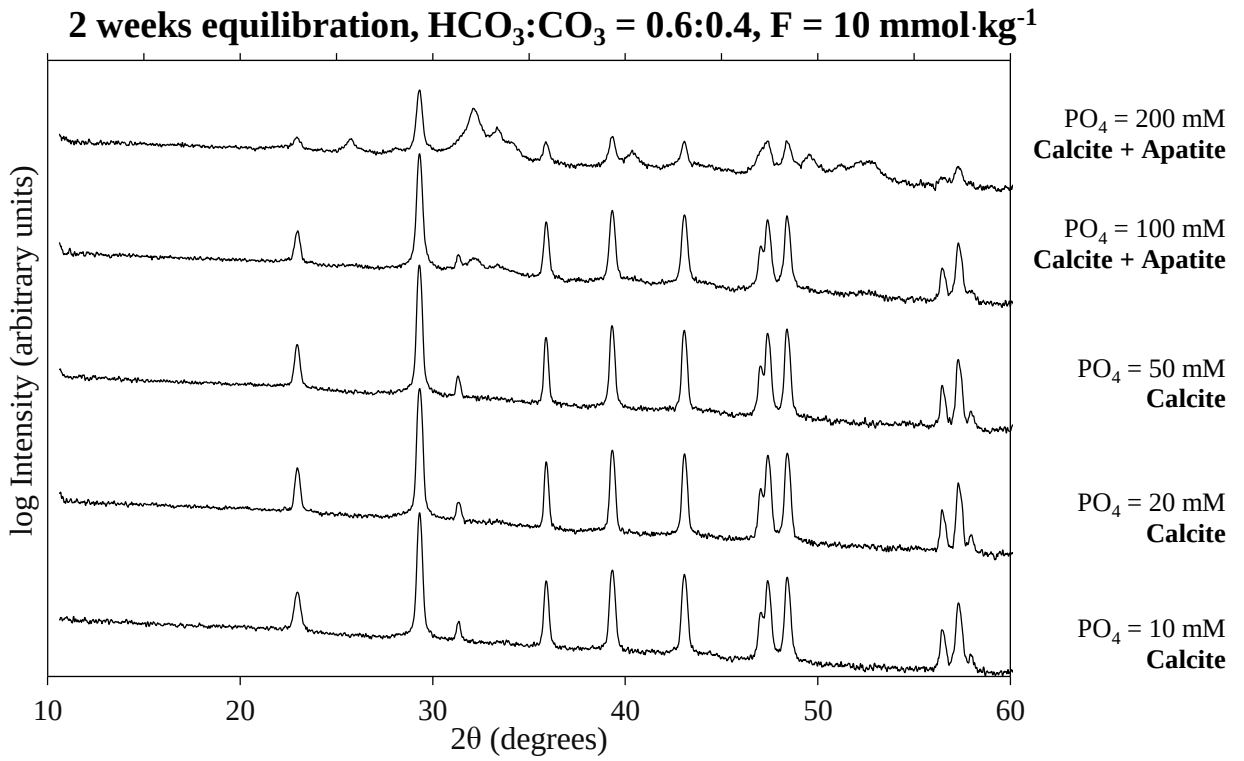


Fig. S6. XRD profiles of saturated carbonate brines with a molar $HCO_3$:$CO_3$ ratio of 0.6:0.4 and 10 mmol·kg$^{-1}$ $F^-$ equilibrated for two weeks at various initial phosphate concentrations. This corresponds to sample numbers 32 to 36 in Table S1 and Table S2.

## Appendix C: Geochemical models

### *The Pitzer model*

To model concentrated solutions in the Na-Cl-P-$CO_2$-H-OH system, we use the Pitzer model (13). The Pitzer equation for the excess Gibbs energy of solution ($G^{EX}$) in a mixed aqueous salt solution containing cations $c$ and anions $a$ is given by:

$$G^{EX} = -4A_\phi \ln\left(1+b\sqrt{I}\right)\frac{I}{b} + \sum_c\sum_a m_c m_a \left(2\beta_{ca} + ZC_{ca}\right) + \sum_c\sum_{c'} m_c m_{c'}\left(2\Phi_{cc'} + m_a\sum_a \psi_{cc'a}\right) + \sum_a\sum_{a'} m_a m_{a'}\left(2\Phi_{aa'} + m_c\sum_c \psi_{aa'c}\right) \quad (1)$$

In this equation, subscript *M* indicates a cation, subscript *X* indicates an anion, *c'* is a cation different from *c*, *a'* is an anion different from *a*, *b* is a constant (1.2 $kg^{-1/2}\cdot mol^{-1/2}$), *I* is the ionic strength given by $I = \frac{1}{2}\sum m_i z_i^{\,2}$, $z_i$ is the ion charge, *Z* is given by $Z = \sum m_i |z_i|$, and $A_\phi$ is the Debye–Hückel limiting law slope. Differentiation of $G^{EX}$ with respect to moles of water ($n_1$) and salt ($n_i$) at molality *m* ($mol\cdot kg^{-1}$) leads to expressions for the activity coefficients for water ($a_w$) and salt ($\gamma$) respectively:

$$\frac{\partial G^{EX}}{\partial n_1} = RT\ln a_w \quad \text{and} \quad \frac{\partial G^{EX}}{\partial n_i} = RT\ln m_i\gamma_i \quad (2)$$

Importantly, water activities are commonly reported as osmotic coefficients ($\phi$), which are related by the equation:

$$\phi = -55.50844\frac{\ln a_w}{\sum m_i} \quad (3)$$

The parameters $\beta$, $C$, and $\Phi$ are given by the functions:

$$\beta_{ca} = \beta_{ca}^{(0)} + \beta_{ca}^{(1)} g(\alpha_1\sqrt{I}) + \beta_{ca}^{(2)} g(\alpha_2\sqrt{I}) \quad (4)$$

$$C_{ca} = \frac{C_{ca}^{\phi}}{2\sqrt{|z_c z_a|}} \quad (5)$$

$$\Phi_{ij} = \theta_{ij} + {}^{E}\theta_{ij} \quad (6)$$

where ${}^{E}\theta_{ij}$ is a higher-order electrostatic terms that account for interactions between ions of the same sign, but different charge (i.e. $z_i \neq z_j$), and $g(x)$ is given by:

$$g(x) = \frac{2\left[1-\left(1+x\right)e^{-x}\right]}{x^2} \quad (7)$$

Finally, equilibrium between an aqueous solution and a hydrated salt with $x$ water molecules, $\nu_c$ cations, and $\nu_a$ anions is described by the precipitation/dissolution reaction:

(8) $$M_{\nu_c}X_{\nu_a}\cdot xH_2O(s) = \nu_c M^{z_c} + \nu_a X^{z_a} + xH_2O$$

where the thermodynamic equilibrium constant $K$ for this reaction may be calculated from the ion activity product of the saturated solution:

(9) $$K = \left(m_c\gamma_c\right)^{\nu_c}\left(m_a\gamma_a\right)^{\nu_a} a_w^x$$

These equations indicate that the Pitzer equations describe properties in mixed electrolyte solutions using the temperature dependent Pitzer parameters $\beta^{(0)}$, $\beta^{(1)}$, $\beta^{(2)}$, $C^{\phi}$, $\theta$, and $\psi$, equilibrium constants $K$, and temperature-invariant parameters $\alpha_1$ and $\alpha_2$. For Pitzer parameters, PHREEQC uses the temperature dependent expression:

(10) $$P = a_0 + a_1\left(\frac{1}{T}-\frac{1}{T_r}\right) + a_2\ln\left(\frac{T}{T_r}\right) + a_3\left(T-T_r\right) + a_4\left(T^2-T_r^2\right) + a_5\left(\frac{1}{T^2}-\frac{1}{T_r^2}\right)$$

where $a_i$ are empirical fitted parameters, $T_r$ is a reference temperature at 298.15 K, and $P$ is a Pitzer parameter. For equilibrium constants, PHREEQC uses the temperature dependent expression:

(11) $$\log K = a_1 + a_2T + \frac{a_3}{T} + a_4\log T + \frac{a_5}{T^2} + a_6T^2$$

***Fits to experimental data on phosphate solubility***

Experimental data on pure saturated sodium phosphate solutions are taken from Seidel (14), and fit to the Pitzer model described above by least-squares-minimization. The experimental data and the resulting model fits are given in Fig. S7.

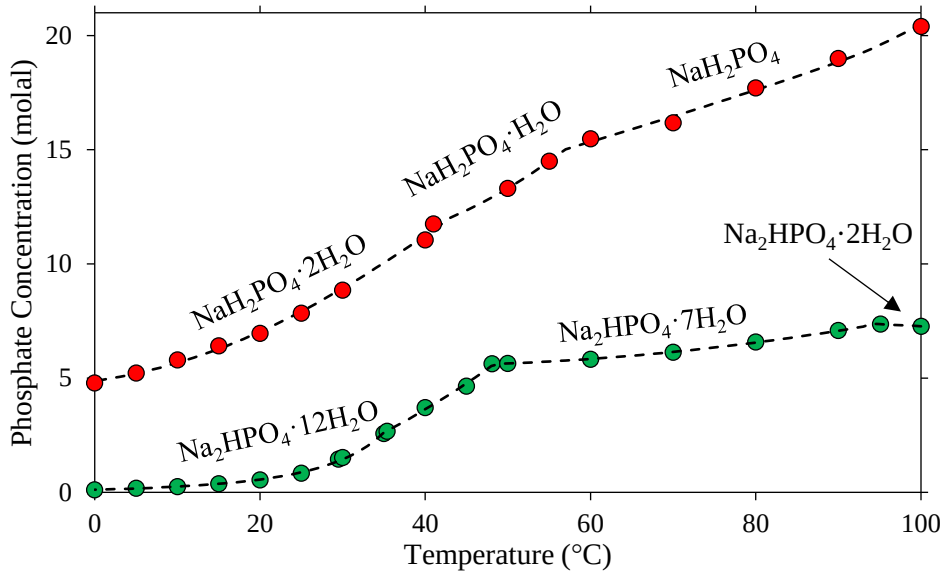


Fig. S7. Experimental solubility measurements (molal) for saturated sodium phosphate solutions at variable temperature for $NaH_2PO_4$ (red circles) and $Na_2HPO_4$ (green circles) salts. The modeled solubility of these salts is given as dashed lines.

***PHREEQC database file***

The following PHREEQC input code was used to model the solubility of phosphate salts in the Na-Cl-P-$CO_2$-H-OH system over a temperature range of 0 to 100°C. The interactive version of PHREEQC is available at https://www.usgs.gov/software/phreeqc-version-3/. If using the interactive version of PHREEQC, the definitions of all input parameters given below are well-described in the program. We have commented on the code primarily to specify the source reference for specific parameters.

```
# Parameters for chloride and carbonate salts and CO2 gas are taken from:
# Marion, G. M., et al. (2011).
# Modeling hot spring chemistries with applications to martian silica formation.
# Icarus 212(2): 629–642.

# Parameters for phosphate salts are taken from:
# Scharge, T., et al. (2013).
# Thermodynamic modelling of high salinary phosphate solutions. I. Binary systems.
# The Journal of Chemical Thermodynamics 64: 249-256.
# Scharge, T., et al. (2015).
# Thermodynamic modeling of high salinary phosphate solutions II. Ternary and higher systems.
# The Journal of Chemical Thermodynamics 80: 172-183.

PITZER
-MacInnes false
-use_etheta true
-redox false

SOLUTION_MASTER_SPECIES
H H+ -1. H 1.008
H(1) H+ -1. 0.0
E e- 0.0 0.0 0.0
O H2O 0.0 O 15.999
O(-2) H2O 0.0 0.0
Na Na+ 0.0 Na 22.99
Cl Cl- 0.0 Cl 35.45
```

```
C CO3-2 2.0 HCO3 12.015
C(4) CO3-2 2.0 HCO3 12.015
P PO4-3 0 94.973 30.973762
P(5) PO4-3 0 94.973

SOLUTION_SPECIES
H+ = H+
 log_k 0

e- = e-
 log_k 0

H2O = H2O
 log_k 0

Na+ = Na+
 log_k 0

Cl- = Cl-
 log_k 0

CO3-2 = CO3-2
 log_k 0

PO4-3 = PO4-3
 log_k 0

H2O = OH- + H+
-analytic -2.2219506201E+02 -5.5058066492E-01 -1.4737247297E+04 1.5156364455E+02 7.7093244810E+05 4.2832724439E-04

CO3-2 + H+ = HCO3-
-analytic 7.8843549125E+01 2.8114156336E-02 -3.5739677566E+03 -2.8384191832E+01 4.7335781578E+05 0

CO3-2 + 2 H+ = CO2 + H2O
-analytic 3.3245684222E+02 7.3424990888E-02 -1.9829264031E+04 -1.1794430937E+02 1.8387797092E+06 0

2H+ + PO4-3 = H2PO4-
 log_k 19.562
 -delta_h -4.520 kcal

3H+ + PO4-3 = H3PO4
 log_k 21.702
 -delta_h -10.1 kJ

H+ + PO4-3 = HPO4-2
 log_k 12.35
 -delta_h -3.530 kcal

PHASES
Halite # From Marion et al. 2011
 NaCl = Cl- + Na+
-analytic -1.2527916896E+02 -1.5940706427E-01 -7.1582997565E+00 6.6592262608E+01 -7.6881371104E-02 1.0843908037E-04

Na2CO3:7H2O # From Marion et al. 2011
 Na2CO3:7H2O = 2Na+ + CO3-2 + 7H2O
-analytic -1.0242414096E+01 3.2849157355E-02 0 0 0 0

Na2CO3:H2O # From Marion et al. 2011
 Na2CO3:H2O = 2Na+ + CO3-2 + H2O
-analytic -2.8774550065E+01 1.8458757574E-01 0 0 0 -2.9016373919E-04

Nahcolite # From Marion et al. 2011
 NaHCO3 = HCO3- + Na+
-analytic 2.7096628475E+02 4.6935820304E-01 1.5642665039E+01 -1.5204447068E+02 1.6854829142E-01 -3.9508831422E-04
```

Natron # From Marion et al. 2011
 Na2CO3:10H2O = CO3-2 + 2 Na+ + 10H2O
-analytic -5.9688261032E+00 -7.4737824292E-03 0 0 0 8.3268627375E-05

Trona # From Marion et al. 2011
 Na3H(CO3)2:2H2O = 3Na+ + HCO3- + CO3-2 + 2H2O
-analytic -1.01750000E+00 1.28307435E-02 -9.59229969E+01 -1.39706624E+00 2.82831158E+03 -8.84486220E-07

Na2(HPO4):12H2O # From this study.
 Na2(HPO4):12H2O = H+ + 12H2O + 2Na+ + PO4-3
 -analytical_expression -81.310371231 0.39641732552 0 0 0 -0.00057403221891

Na2(HPO4):7H2O # From this study.
 Na2(HPO4):7H2O = 7H2O + HPO4-2 + 2Na+
 -analytical_expression -53.300652324 0.31115586643 0 0 0 -0.00046145146621

Na2(HPO4):2H2O # From this study.
 Na2(HPO4):2H2O = 2H2O + HPO4-2 + 2Na+
 -analytical_expression 9.7729128374 -0.059178506134 0 0 0 8.4416737735e-05

Na2(HPO4) # From this study.
 Na2(HPO4) = HPO4-2 + 2Na+
 -analytical_expression 13.896733053 -0.059661090262 0 0 0 5.7293521435e-05

Na(H2PO4):2H2O # From this study.
 Na(H2PO4):2H2O = 2H+ + 2H2O + Na+ + PO4-3
 -analytical_expression -10.856644409 -0.082448426323 0 0 0 0.00018313420267

Na(H2PO4):H2O # From this study.
 Na(H2PO4):H2O = 2H+ + H2O + Na+ + PO4-3
 -analytical_expression 46.342978362 -0.43751747619 0 0 0 0.00073603174603

Na(H2PO4) # From this study.
 Na(H2PO4) = 2H+ + Na+ + PO4-3
 -analytical_expression -17.735301819 -0.0278227 0 0 0 8.6142857143e-05

CO2(g) # From Marion et al. 2011
 CO2 = CO2
-analytic 7.6172730397E+01 1.4954581339E-02 -5.1694861624E+03 -2.8759485533E+01 5.6914636107E+05 0.0000000000E+00

PITZER
-B0
# The following are from Marion et al. 2011
H+ Cl- 1.9794612033E-01 4.3930392007E-02 2.6162364573E-04 -5.3121505493E-04 3.4074178888E-10 -1.3794988905E+00
Na+ Cl- 7.6273259396E-02 -1.0677687696E+03 -5.2850452529E+00 9.0310652648E-03 -2.5394712901E-06 1.4568462343E+04
Na+ CO3-2 3.6204808669E-02 1.1083789213E+03 1.1198570286E+01 -2.3301689083E-02 1.4225931266E-11 -1.0139889781E-01
Na+ HCO3- 2.8002054979E-02 6.8287100127E+02 6.8994999437E+00 -1.4459103667E-02 -1.0139500105E-10 4.8617733194E-01
Na+ OH- -7.9555220526E-02 2.0309032437E+04 1.6146658627E+02 -5.2616228562E-01 2.9653500975E-04 -5.1829489159E+05
# The following are from Scharge et al. 2013, 2015
Na+ H2PO4- -0.0436
Na+ HPO4-2 -0.0172
Na+ PO4-3 0.15641

-B1
# The following are from Marion et al. 2011
H+ Cl- 1.7663995597E-01 -4.4613022946E+04 -3.1259930375E+02 9.5812792829E-01 -5.3080804721E-04 1.2316610809E+06
Na+ Cl- 2.8041722849E-01 -4.7934459033E+03 -6.9757728955E+01 2.2182662176E-01 -1.0800038619E-04 -3.1269129963E+05
Na+ CO3-2 1.5120691287E+00 4.4124805360E+03 4.4581885679E+01 -9.9890728880E-02 -2.3470887122E-10 1.0021144087E+00
Na+ HCO3- 4.4005226296E-02 1.1292842314E+03 1.1410242105E+01 -2.4464729852E-02 -7.4828259687E-10 3.3354784151E+00
Na+ OH- 2.5311163491E-01 1.4885507672E+04 1.1834672330E+02 -3.9540544436E-01 2.3380756117E-04 -3.7988491809E+05
# The following are from Scharge et al. 2013, 2015
Na+ H2PO4- -0.03389
Na+ HPO4-2 1.2116
Na+ PO4-3 3.9397

-C0
# The following are from Marion et al. 2011
H+ Cl- -2.8913465588E-03 1.0693004789E-02 5.5410207932E-05 1.7224827506E-05 -5.9323763662E-08 -3.7953644554E-01
Na+ Cl- 1.2711016441E-03 7.7695148783E+01 2.3007504621E-01 -8.0897946811E-05 -1.1941587694E-07 -2.0177121991E+03
Na+ CO3-2 0.0052
Na+ OH- 4.1159992172E-03 7.3302950838E+02 5.8279924019E+00 -2.0502290395E-02 1.2873934762E-05 -1.8707050080E+04
# The following are from Scharge et al. 2013, 2015
Na+ H2PO4- 0.00605
Na+ HPO4-2 0.00585
Na+ PO4-3 -0.03498

-LAMDA
# The following are from Marion et al. 2011
Cl- CO2 2.0480415080E-02 -3.3159597997E+04 -3.1582776282E+02 9.9643227553E-01 -5.2121983640E-04 -6.0314596673E-01
Na+ CO2 8.1474353447E-02 1.0939930101E+05 1.0470213325E+03 -3.3265653899E+00 1.7531997031E-03 1.2758007796E+00

-PSI
# The following are from Marion et al. 2011
Cl- CO3-2 Na+ 8.6555626983E-03 -1.1578726767E+01 -1.1401251201E-01 4.4733586264E-04 -4.6816398956E-07 3.7067215792E+02
Cl- HCO3- Na+ -1.2777037089E-02 -1.1975486345E+01 -1.4023338938E-01 5.1084176969E-04 -5.9489945059E-07 4.5438567976E+02
Cl- OH- Na+ -0.006
HCO3- CO3-2 Na+ 0.002
Na+ H+ Cl- -0.0037
OH- CO3-2 Na+ -0.017
# The following are from Scharge et al. 2013, 2015
Cl- H2PO4- Na+ -0.01208
Cl- HPO4-2 Na+ -0.00883
Cl- PO4-3 Na+ -0.00243
HPO4-2 H2PO4- Na+ 0.03781
PO4-3 HPO4-2 Na+ 0.00207
CO3-2 PO4-3 Na+ -0.01449774

-THETA
# The following are from Marion et al. 2011
Cl- CO3-2 -0.02
Cl- HCO3- 0.03
Cl- OH- -0.05
HCO3- CO3-2 -0.04
Na+ H+ 0.036
OH- CO3-2 0.1
# The following are from Scharge et al. 2013, 2015
Cl- H2PO4- 0.10037
Cl- HPO4-2 0.07083
Cl- PO4-3 0.24341
H2PO4- HPO4-2 -0.32361
PO4-3 HPO4-2 0.25528
CO3-2 PO4-3 0.19766089

-ZETA
# The following are from Marion et al. 2011
H+ Cl- CO2 -4.7051879034E-03 1.6334349475E+04 1.5238364378E+02 -4.7047340910E-01 2.4052572265E-04 1.2740734776
Na+ Cl- CO2 -5.7153028547E-04 6.87905500E+03 7.3745255829E+01 -2.58005360E-01 1.4782317370E-04 -7.78048610E-01

-APHI
# The following are from Marion et al. 2011
3.9147193099E-01 3.6897938637E+02 3.5956550857E+00 -1.2908353094E-02 9.5199168775E-06 4.7098725794E+01

## Supplementary References


1. Eugster HP & Jones BF (1979) Behavior of major solutes during closed-basin brine evolution. *American Journal of Science* 279(6):609-631.
2. Smith GI & Stuiver M (1979) Subsurface stratigraphy and geochemistry of late Quaternary evaporites, Searles Lake, California. *Geological Survey Professional Paper* 1043:1-130.
3. Friedman I, Smith GI, & Hardcastle KG (1976) Studies of quaternary saline lakes—II. Isotopic and compositional changes during desiccation of the brines in Owens Lake, California, 1969–1971. *Geochim. Cosmochim. Acta* 40(5):501-511.
4. Felmy AR & Weare JH (1986) The prediction of borate mineral equilibria in natural waters: Application to Searles Lake, California. *Geochim. Cosmochim. Acta* 50(12):2771-2783.
5. Grew ES, Bada JL, & Hazen RM (2011) Borate minerals and origin of the RNA world. *Origins of Life and Evolution of Biospheres* 41(4):307-316.
6. Hirst JF (2013) Sedimentology, diagenesis and hydrochemistry of the saline, alkaline lakes on the Cariboo Plateau, Interior British Columbia, Canada. Ph.D. (University of Saskatchewan, Saskatoon).
7. Clarke FW (1924) The composition of the river and lake waters of the United States. *US Government Printing Office* 135.
8. Felmy AR, Dixon DA, Rustad JR, Mason MJ, & Onishi LM (1998) The hydrolysis and carbonate complexation of strontium and calcium in aqueous solution. Use of molecular modeling calculations in the development of aqueous thermodynamic models. *J. Chem. Thermodyn.* 30(9):1103-1120.
9. Jones BE, Grant WD, Duckworth AW, & Owenson GG (1998) Microbial diversity of soda lakes. *Extremophiles* 2(3):191-200.
10. Eugster HP & Hardie LA (1978) Saline lakes. *Lakes*, (Springer, New York), pp 237-293.
11. Mochizuki A*, et al.* (2018) Distribution of trace elements and the influence of major-ion water chemistry in saline lakes. *Limnology and Oceanography* 63(3):1253-1263.
12. Feldman I (1956) Use and abuse of pH measurements. *Anal. Chem.* 28(12):1859-1866.
13. Pitzer KS (1991) Ion interaction approach: Theory and data correlation. *Activity Coefficients in Electrolyte Solutions*, (CRC Press, Boca Raton), second Ed, pp 75–153.
14. Seidell A (1919) *Solubilities of inorganic and organic compounds* (D. Van Nostrand Company).